NAVAL POSTGRADUATE SCHOOL

MONTEREY, CALIFORNIA

THESIS

RESOLVING BEARING AMBIGUITY WITH A SINGLE BIO-INSPIRED DIRECTION FINDING MEMS ACOUSTIC SENSOR

by

Brian Gureck

June 2020

Thesis Advisor: Gamani Karunasiri
Co-Advisor: Fabio D. Durante Pereira Alves

THIS PAGE INTENTIONALLY LEFT BLANK

REPORT DOCUMENTATION PAGE			*Form Approved OMB No. 0704-0188*

1. AGENCY USE ONLY *(Leave blank)*	**2. REPORT DATE** June 2020	**3. REPORT TYPE AND DATES COVERED** Master's thesis

4. TITLE AND SUBTITLE RESOLVING BEARING AMBIGUITY WITH A SINGLE BIO-INSPIRED DIRECTION FINDING MEMS ACOUSTIC SENSOR	**5. FUNDING NUMBERS** RPN07; RPMY8
6. AUTHOR(S) Brian Gureck	
7. PERFORMING ORGANIZATION NAME(S) AND ADDRESS(ES) Naval Postgraduate School Monterey, CA 93943-5000	**8. PERFORMING ORGANIZATION REPORT NUMBER**
9. SPONSORING / MONITORING AGENCY NAME(S) AND ADDRESS(ES) Space & Naval Warfare Systems Center-Pacific, San Diego, CA 92110; Office of Naval Research, Arlington, VA 22203	**10. SPONSORING / MONITORING AGENCY REPORT NUMBER**

11. SUPPLEMENTARY NOTES The views expressed in this thesis are those of the author and do not reflect the official policy or position of the Department of Defense or the U.S. Government.

12a. DISTRIBUTION / AVAILABILITY STATEMENT Approved for public release. Distribution is unlimited.	**12b. DISTRIBUTION CODE** A

13. ABSTRACT (maximum 200 words)

Microelectromechanical systems (MEMS) based directional sound sensors have been developed to mimic the unique hearing mechanism of the parasitoid fly *Ormia ochracea.* The fly appears to analyze the superposition of the two natural oscillation modes (rocking and bending) of the coupled eardrums to identify the incident direction of the cricket chirp. This approach allows it to accurately determine the direction of sound using wavelengths that are much longer than the gap between the fly's hearing organs. The sensor developed by NPS consists of two wings that are attached to a substrate using two torsional legs at the middle, as detailed in several previous theses. The current detection systems based on the fly's hearing system requires two sensors to uniquely determine the direction since only one mode is utilized. This study focuses on the use of a single MEMS sensor by analyzing the superposition of the rocking and bending modes in order to produce a sensor that directly mimics the parasitoid fly while reducing the overall size of the device. The measurements show that signals from the two wings can be processed to uniquely determine the direction of sound. In addition, the measurements agreed with that of simulations utilizing finite element modeling. The findings indicate that MEMS based sensors having dimensions much smaller than the wavelength of sound they detect can be developed to accurately determine the bearing of incident sound.

14. SUBJECT TERMS MEMS, acoustic, narrowband detection, sensor, parasitoid fly, bearing ambiguity, capacitive, biomimetic, sound source localization	**15. NUMBER OF PAGES** 73
	16. PRICE CODE

17. SECURITY CLASSIFICATION OF REPORT	**18. SECURITY CLASSIFICATION OF THIS PAGE**	**19. SECURITY CLASSIFICATION OF ABSTRACT**	**20. LIMITATION OF ABSTRACT**
Unclassified	Unclassified	Unclassified	UU

NSN 7540-01-280-5500 Standard Form 298 (Rev. 2-89) Prescribed by ANSI Std. 239-18

THIS PAGE INTENTIONALLY LEFT BLANK

Approved for public release. Distribution is unlimited.

RESOLVING BEARING AMBIGUITY WITH A SINGLE BIO-INSPIRED DIRECTION FINDING MEMS ACOUSTIC SENSOR

Brian Gureck
Lieutenant, United States Navy
BS, United States Naval Academy, 2013

Submitted in partial fulfillment of the
requirements for the degree of

MASTER OF SCIENCE IN APPLIED PHYSICS

from the

NAVAL POSTGRADUATE SCHOOL
June 2020

Approved by: Gamani Karunasiri
Advisor

Fabio D. Durante Pereira Alves
Co-Advisor

Kevin B. Smith
Chair, Department of Physics

THIS PAGE INTENTIONALLY LEFT BLANK

ABSTRACT

Microelectromechanical systems (MEMS) based directional sound sensors have been developed to mimic the unique hearing mechanism of the parasitoid fly *Ormia ochracea.* The fly appears to analyze the superposition of the two natural oscillation modes (rocking and bending) of the coupled eardrums to identify the incident direction of the cricket chirp. This approach allows it to accurately determine the direction of sound using wavelengths that are much longer than the gap between the fly's hearing organs. The sensor developed by NPS consists of two wings that are attached to a substrate using two torsional legs at the middle, as detailed in several previous theses. The current detection systems based on the fly's hearing system requires two sensors to uniquely determine the direction since only one mode is utilized. This study focuses on the use of a single MEMS sensor by analyzing the superposition of the rocking and bending modes in order to produce a sensor that directly mimics the parasitoid fly while reducing the overall size of the device. The measurements show that signals from the two wings can be processed to uniquely determine the direction of sound. In addition, the measurements agreed with that of simulations utilizing finite element modeling. The findings indicate that MEMS based sensors having dimensions much smaller than the wavelength of sound they detect can be developed to accurately determine the bearing of incident sound.

THIS PAGE INTENTIONALLY LEFT BLANK

TABLE OF CONTENTS

THIS PAGE INTENTIONALLY LEFT BLANK

LIST OF FIGURES

THIS PAGE INTENTIONALLY LEFT BLANK

LIST OF ACRONYMS AND ABBREVIATIONS

FE	Finite Element
LDV	Laser Doppler Vibrometry
MEMS	Microelectromechanical systems
mIPD	Mechanical Interaural Phase Difference
NPS	Naval Postgraduate School
PCB	Printed Circuit Board
SOI	Silicon-on-Insulator
SOIMUMPs	Silicon-on-Insulator Multi User Manufacturing Process
UV	Ultraviolet

THIS PAGE INTENTIONALLY LEFT BLANK

ACKNOWLEDGMENTS

I could not have achieved any success in this project without the incredible leadership and knowledge from my advisors, Dr. Gamani Karunasiri and Dr. Fabio Alves. Dr. Karunasiri's deep understanding of the subject and his vision to propel the project forward was instrumental in the progress made by the entirety of our research group. Dr. Alves was a wealth of technical prowess and innovation, never ceasing to surprise us all with a new design or function he produced seemingly out of thin air.

I would also like to thank Dr. Renato Rabelo for his unwavering technical assistance and for fielding an onslaught of daily questions that were always met with insightful and critical answers that allowed this project to achieve great success.

This research would not have been possible without the generous funding and support through the Naval Information Warfare Center (NIWC) Pacific NPS Research Fellowship program and the Office of Naval Research (ONR).

I am forever grateful to my wife, McKalie, for her patience, support, and encouragement during these years in Monterey. She has been my rock since day one and our time here in Monterey was no exception. This goal would never have been possible without her love and devotion to our family. As for my son, Mason, I did this for you. Learn something new each and every day and never stop achieving your dreams.

THIS PAGE INTENTIONALLY LEFT BLANK

I. INTRODUCTION

A. BACKGROUND

In the defense community, there exists a desire to detect the direction of sound from several sources using small, low-power consumption sensors. This technology would provide the user with the incoming direction of hostile targets or projectiles with a high degree of accuracy using a device that is small enough to be used as a wearable detection system. The Naval Postgraduate School (NPS) is working to fulfil this need with biomimetic Microelectromechanical systems (MEMS) devices to provide directional localization of sound sources.

1. MEMS Acoustic Directional Sensors

In 1995, Miles et al. [1] studied and identified the natural resonant frequency modes of oscillation of the parasitic fly *Ormia ochracea* by analyzing the mechanical nature of the fly's hearing organ (see Figure 1). Miles demonstrated that the eardrum of the fly could be easily modeled using a simple mechanical structure consisting of two bars connected by a central flexible pivot which excites at two distinct oscillation frequencies, a rocking and bending frequency. The fly is able to locate the incident angle of a cricket chirp by comparing the superposition of the natural oscillation modes despite the cricket chirp wavelength being nearly two orders of magnitude larger than the size of the fly's hearing organ.

For several decades, MEMS devices have been utilized as acoustic directional sensors. *Ormia*-based MEMS are typically designed to operate at either the rocking or bending natural frequency oscillation modes [2]. Many researchers utilize the higher amplitude of the bending mode to design a pressure gradient microphone in order to discern incident direction of sound [2], [3]. Few researchers are also designing their MEMS directional sensors to optimize the rocking mode of the MEMS device [2]. Additionally, the superposition of coupling the rocking and bending vibration modes to determine the incident direction of sound is being explored [4], [5].

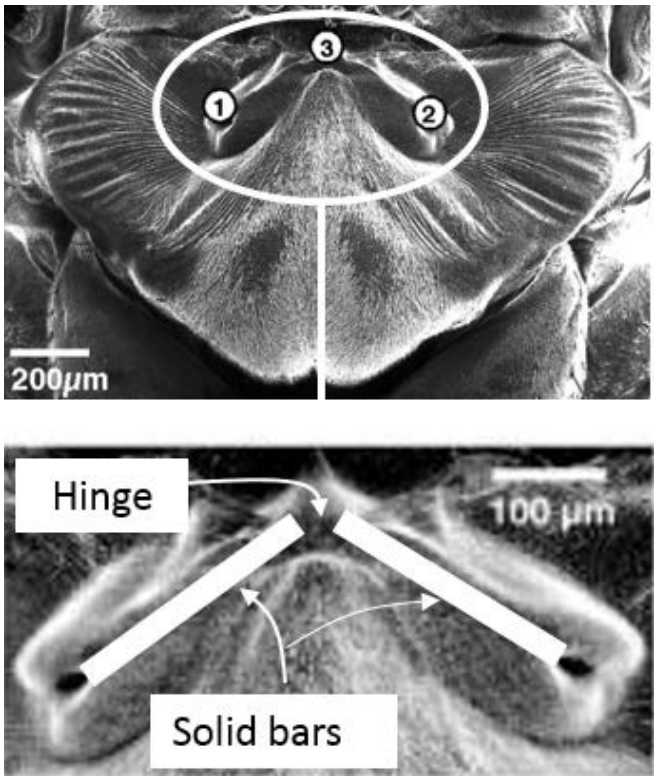

Components 1 and 2 are the tympanal membranes of the fly. Component 3 is the cartilaginous bridge that connects the two tympanal membranes and acts as a pivot for the oscillatory mechanical structure.

Figure 1. Hearing Organ of *Ormia Ochracea* with Highlighted Components. Source: [1].

In a paper published for the MEMS 2006 Conference, Cui et al. [3] demonstrated the fabrication and characterization of an *Ormia*-based MEMS directional sound sensor using a diffraction-based optical readout. Inter-digitated comb fingers at the sensor edges allowed for optical interferometric detection of sensor motion. Incident sound on the sensor caused the device to pivot about its hinges when excited at a frequency corresponding to the rocking mode of the sensor. In this manner, the device acts as a pressure gradient microphone and the difference in amplitude of the rocking mode with angle is utilized to determine direction of sound. Thus, the sensor demonstrates a nearly ideal figure-8 pattern when rotated in-plane and produces a 21.9 dB difference in sound signal between the minima and maxima of the response [3].

Liu et al. [4] designed an optical fiber based microphone that mimicked the coupling of the rocking and bending modes of an *Ormia*-based mechanical structure. The design used two circular membranes that are connected with a coupling bridge that acts as the pivot. The mechanical deflection of the circular membranes are sensed with a fiber optic interferometer that was chosen for its high sensitivity and resolution with low noise. In order to determine the direction of incident sound, Liu et al. make use of the mechanical interaural phase difference (mIPD) between the two circular membranes. The MEMS device was able to locate a sound source with a localization accuracy better than ±2º within a range of $-30° \leq \theta \leq 30°$. These metrics were achieved when the sensor was able to rotate in response to the incoming signal to localize the sound source vice the sensor being stationary and detecting the incoming direction of sound [4].

Utilizing a disc-based MEMS design, Mackie et al. [5] achieved an unambiguous determination of direction of arrival of incident sound from $-75° \leq \theta \leq 60°$. Their design consisted of two unclamped circular plates connected via a flexible bridge with an open backside. It was stimulated at a frequency that exhibited an interaction between the rocking and bending modes which generated an overall superposition of wing deflection that was predicted by Finite Element (FE) modeling and measured by Laser Doppler vibrometry (LDV). Overall, they achieved an unambiguous determination of the angle of the sound source over a range of 130° based on the amplitude of the deflected diaphragm [5].

Unlike most of the directional MEMS acoustic sensors being explored to date, the MEMS sensor created at NPS will explore the superposition of the rocking and bending vibration modes in order to resolve directional ambiguity. Due to the superposition of the two modes of oscillation, the deflection of each wing will correspond to a unique angle of incidence thereby resolving the directional ambiguity that comes with the normal figure-8 pattern that is seen with pressure gradient sensors.

2. NPS MEMS Sensor

The simple mechanical structure proposed by Miles et al. [1] can be mimicked using a MEMS device only a few millimeters in size. The tympanal membranes and cartilaginous bridge of the *Ormia* fly are replicated using a silicon layer consisting of two

wings with a flexible bridge. The devices used at NPS were produced by MEMSCAP utilizing the Silicon-on-Insulator Multi User Manufacturing Process (SOIMUMPs) on a Silicon-on-Insulator (SOI) wafer 400 microns thick with a 25 micron device layer [6]. Figure 2 shows an optical micrograph of the sixth generation of sensors developed at NPS. The device consists of two wings connected by a flexible bridge. The connection of the wings to the bridge is in the interior of the wings and found to reduce the residual stress related warp of the wings after MEMS fabrication [7]. The bridge is connected to the substrate via two torsional legs that act as the pivot for the bridge. The backside of the substrate is chemically etched entirely to the device layer to allow the wings to move freely when subject to incident sound excitation.

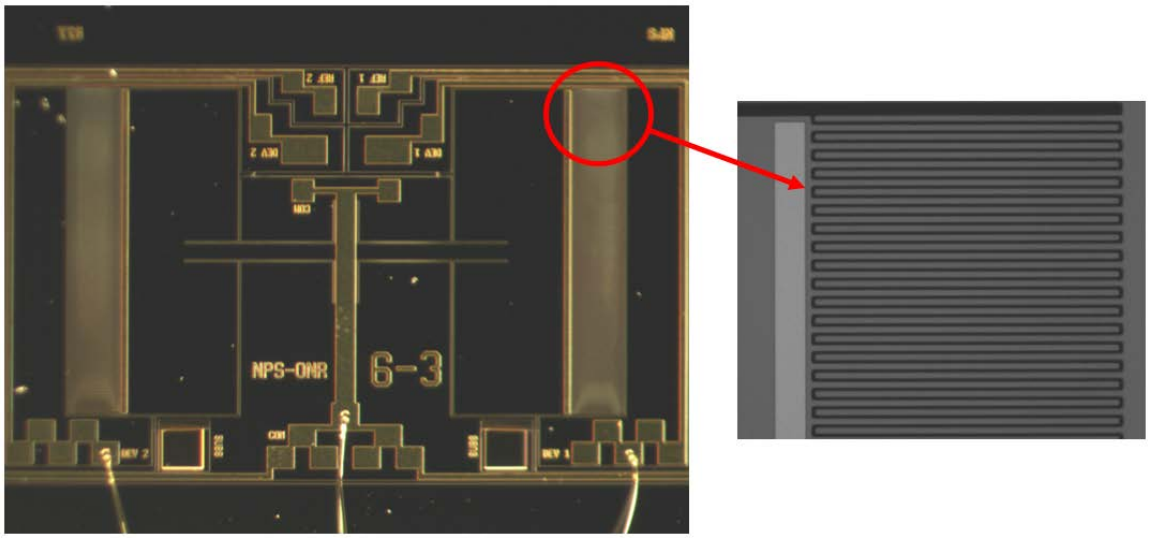

Figure 2. Optical Micrograph of MEMS Acoustic Sensor with Corresponding Image of Interdigitated Comb Fingers

In order to extract the mechanical displacement of the sensor into a useable electrical signal, comb fingers are placed at the wing's edge, as shown in Figure 2. The comb fingers on the wing tips are interdigitated to the stationary comb fingers that are attached to the substrate. The comb fingers generate a capacitance value proportional to the deflection of each wing caused by sound excitation. In order to analyze the

superposition of the oscillation modes, each wing must be read individually which can be done using a charge amplifier circuit.

In previous designs of MEMS sensors [7], [8], the back side of the sensor has been left open during the measurements. This allows for the sensor to act as a pressure gradient microphone where the pressure difference generated is a function of the extra distance required for the sound waves to travel to impact the front and back sides of the sensor. This has been shown to have a cosine dependence on incident angle of sound as shown in Figure 3 [9]. When the sound is at normal incidence, the bending amplitude is at a maximum and when the sound is at 90 degrees (parallel to the wings), the bending amplitude is zero since the pressure on both sides of the wings is the same. It can be seen in the angular response of the sensor in Figure 3 that there is a bearing ambiguity between the left and right sides. The left and right ambiguity can be resolved by using two sensors that are canted as shown in Figure 4 that was studied by Wilmott. In these measurements, the rocking mode was essentially not included and response at the bending mode was measured to determine the incident direction of sound over a 120-degree detection range [7].

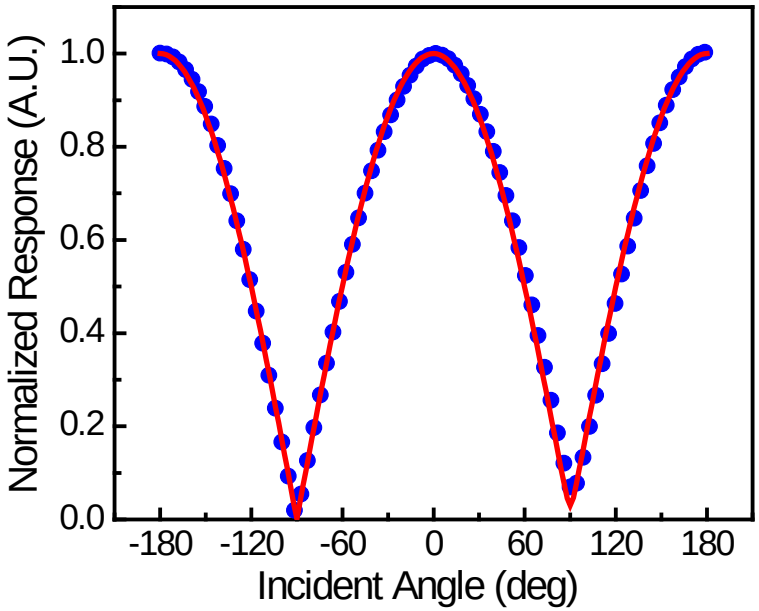

Figure 3. Experimental (blue) and FE (red) Results of the Directional Response of Sensor with Open Backside at Rocking Frequency. Source: [9].

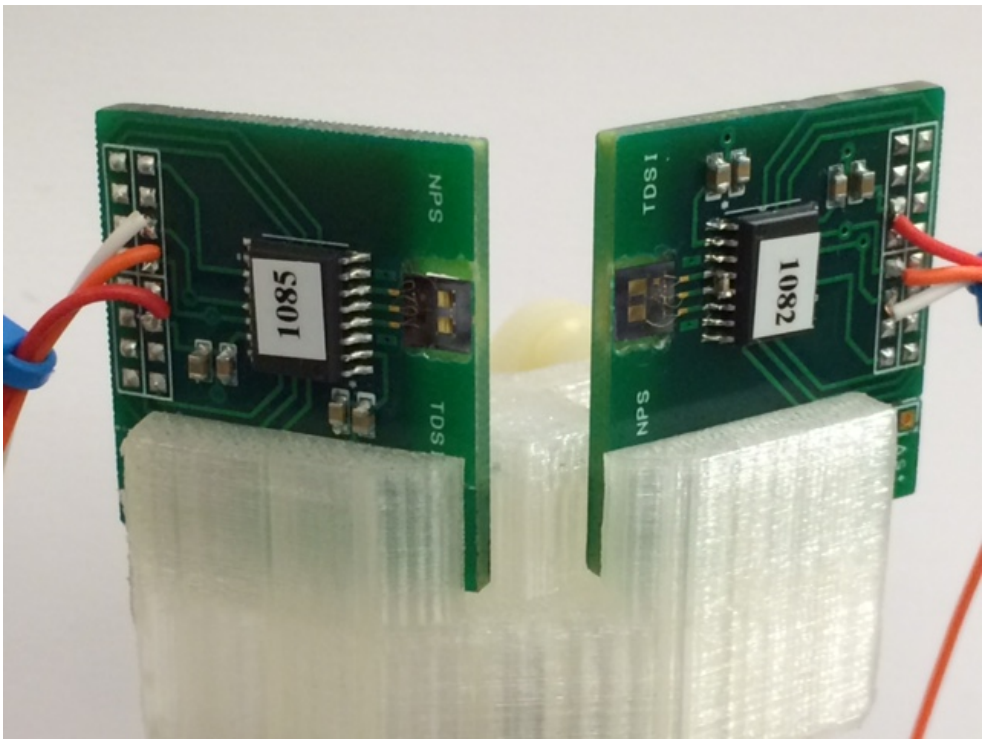

Figure 4. Fabricated Dual Sensor Assembly for Resolving Directional Ambiguity. Source: [9].

B. OBJECTIVE AND THESIS ORGANIZATION

The purpose of this study is to utilize the superposition of the two natural oscillation modes observed in the *Ormia Ochracea* fly to achieve unambiguous determination of incident sound over a 180° range with maximum sensitivity using a single sensor. The superposition of the two modes will be controlled by closing the backside of the MEMS directional acoustic sensor and controlling the magnitude of damping.

This thesis is organized into four chapters. Chapter I provided an introduction to the MEMS directional acoustic sensor inspired by the *Ormia Ochracea* fly, previous research conducted on the subject, and the basis for the current design of the NPS sensor.

Chapter II details the methodology behind the current NPS sensor and the overall design and implementation of the experiment. Finite Element (FE) design, simulations, and the design and fabrication of the sensor are included.

Chapter III contains the experimental measurements obtained in the anechoic chamber and a discussion on the results obtained.

Chapter IV demonstrates the benefits of optimizing the geometry of the sensor using FE simulations. Chapter V contains an analysis on the relative success of the results of this study and recommendations for future work.

THIS PAGE INTENTIONALLY LEFT BLANK

II. MODELING AND SIMULATION

The MEMS directional acoustic sensor described in this thesis was inspired by the ability of the *Ormia Ochracea* parasitic fly to locate and direction find a distinct cricket chirp frequency that was first described by Miles et al. [1]. His research demonstrated the fly's hearing organ is excited at two natural frequencies corresponding to a rocking and a bending oscillation mode as illustrated schematically in Figure 5 using a simple mechanical structure. The rocking mode is a function of the time difference of arrival of the incident sound wave upon the two tympanal membranes and gives directional sensitivity to the sensor while causing the membranes to move in opposite directions. The bending mode is due to the pressure of the sound wave on the tympanal membranes and causes the membranes to move in the same direction as each other. The motion of membranes or wings in the case of a MEMS directional acoustic sensor, can be modeled as superposition of the two modes providing unequal displacements on the two sides depending on the direction of sound (see Figure 5).

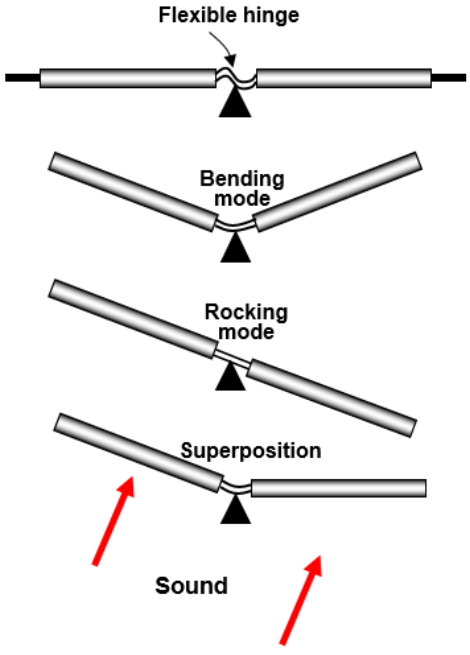

Figure 5. Mechanical Structure Showing Response of Natural Oscillation Modes to Incident Sound

In order to create a MEMS directional acoustic sensor that can determine the direction of incident sound while resolving left and right ambiguity, the superposition of the rocking and bending modes must be analyzed. From Figure 5, it can be shown that when excited by an incident sound wave, the mechanical structure will generate a superposition of the two natural oscillation modes if at a distinct frequency, both modes are present. Both the rocking and the bending mode will deflect in the same direction on the ipsilateral side resulting in a greater net deflection of the ipsilateral wing. Conversely, the contralateral wing will experience a net decrease in deflection when the rocking and bending modes cause the wing to move in opposing directions. The ability to control the amplitude of the two modes of oscillation at a given frequency and optimize their resulting superposition into a usable electronic readout is the objective of this study.

As mentioned, when the backside of the MEMS directional acoustic sensor is left open, the bending mode dominates the rocking mode by an order of magnitude and the sensor acts as a pressure gradient microphone [10]. In this configuration, the superposition of the two modes would resemble the directional response of the bending mode which does not contain the directional response data from the time difference of arrival of incident sound. To achieve proper superposition of the modes, the amplitude of the bending mode needs to be reduced and the full width at half maximum (FWHM) broadened which can be accomplished by enclosing the air cavity behind the sensor wings as illustrated in Figure 20. The bending mode is reduced due to the elimination of coupling of sound from the backside as well as increased damping as it tries to squeeze the air volume behind the wings. The rocking mode remains unaffected as it experiences no net change in the volume of air in the cavity. In this manner, the bending mode amplitude can be controlled to determine the optimum amplitude of each mode present at a given frequency. In order to control the amount of damping applied to the bending mode, a hole is drilled into the backside of the enclosure (see Figure 19). If there was no hole present, the bending mode of the wings would theoretically be completely damped and only the rocking mode would remain. In practice, however, this would not be the case as the air can escape out the front side of the device layer through the gaps between the interdigitated comb fingers and the other gaps around the moving parts of the sensor.

The effect of closing the backside of the cavity was briefly studied by Wilmott [7] who demonstrated that enclosing the backside of the sensor allows for a MEMS directional acoustic sensor that more closely mimics that of the *Ormia* fly. He showed that damping the bending mode of oscillation by these means was effective at coupling the two modes and use it for acoustic direction finding. However, the electronics used for Wilmott's research prevented him from being able to read each wing independently which is a required analysis for determining the superposition of the two oscillation modes. Riarh further studied the effects of closing the backside on the sensor and although was able to achieve unambiguous incident angle determination over a range of about 120° [11], was also limited by the capacitive readout electronics being used at that time. Both Wilmott and Riarh were not able to measure both wings simultaneously, which does not allow for the potential of a full range of detection of 180°. The following research is conducted with a charge amplifier circuit that was specifically designed for simultaneous measurements of signals from both wings independently.

By controlling the geometry of the MEMS directional acoustic sensor, the rocking and bending mode peak frequencies and amplitudes can be tuned to a desired value. If the two oscillation modes of the sensor occur at frequencies that are too distant from each other, the two modes will act independently and there will be no superposition. Without the superposition of the two modes, a single sensor would not be able to resolve the left and right ambiguity of the response. A MEMS sensor was designed and fabricated to properly overlap the two oscillation modes at a narrow band of frequencies within the audible range. The sensor consists of two wings that are 1095 μm by 3000 μm in area as shown in Figure 6. They are connected to each other via a 3000 μm bridge that acts as the flexible hinge. Perpendicular to the center of the bridge are two 400 μm long and 200 μm wide torsional legs that connect the wings and bridge to the fixed substrate. The bridge extends 500 μm into each wing to reduce the residual stress induced warp of the wings during fabrication [12]. The comb fingers used for electronic readout are each 500 μm long and 10 μm wide. There is a 5 μm gap between each of the comb fingers. The sensor dimensions are shown on a micrograph of the sensor in Figure 6 and Figure 7 shows a magnified view of the combs. The entire structure of the sensor with the exception of the

two points where the torsional legs attach to the substrate is surrounded by a 20 µm gap between the moving portion of the sensor and the rest of the substrate.

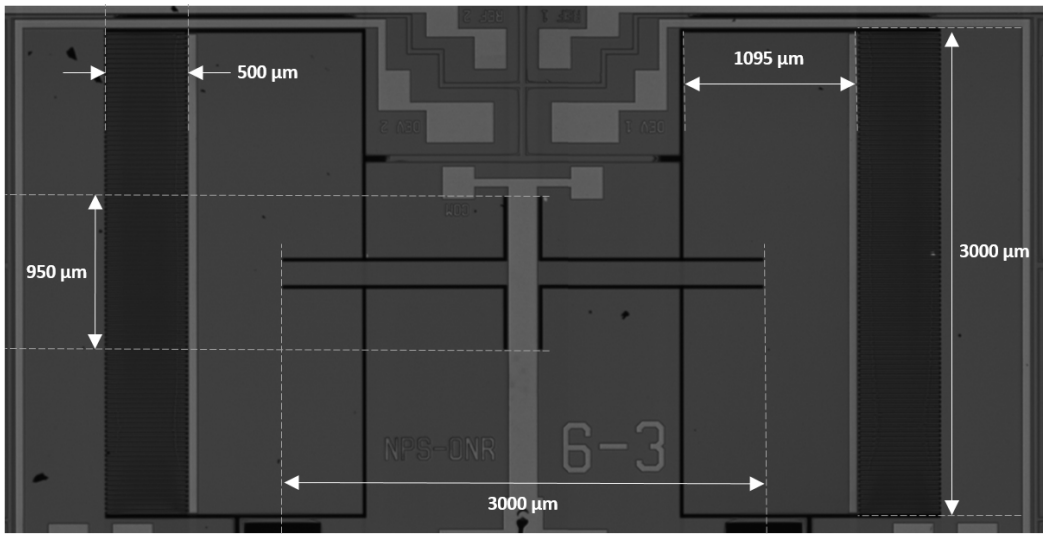

Figure 6. Optical Micrograph of MEMS Acoustic Sensor with Major Dimensions (Gen 6–3 Sensor)

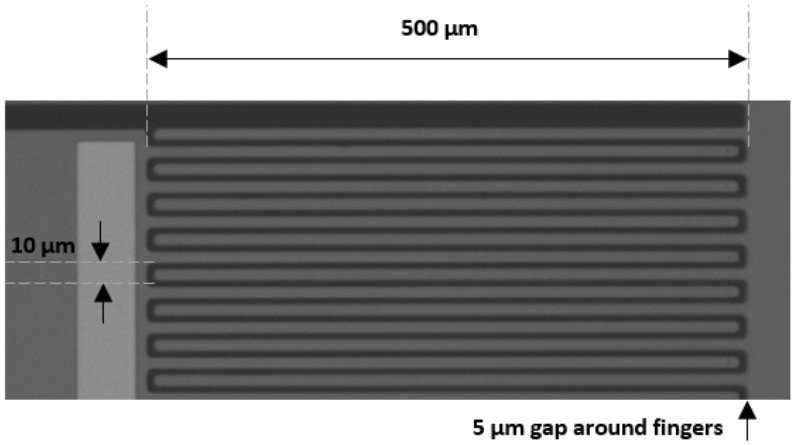

Figure 7. Optical Micrograph of Comb Fingers with Dimensions

In order to characterize the response of the sensor, FE simulations were conducted using COMSOL Multiphysics software [13]. The simulation employed the solid mechanics, pressure acoustics, and thermoviscous acoustics physics models. The geometry of the MEMS sensor shown in Figure 6 was generated within the software. A sphere of air

is modeled around the MEMS sensor to mimic the atmosphere and a plane wave at 1 Pa is applied towards the sensor at a specified angle of incidence. This allows for normalizing the deflection amplitude in terms of [units] per Pa. The sensor is modeled on top of the printed circuit board (PCB) as it will be placed in the experimental setup. Behind the sensor, the PCB has a hole where the sensor sits to allow for sound waves to act on both sides of the sensor. Following analysis on the open back configuration, a back plate is included in the model with a varying hole size to control the damping of the overall sensor.

Two main studies were conducted using COMSOL with the MEMS directional acoustic sensor. The first consisted of a mechanical frequency response over a range of frequencies. At each frequency, the deflection of the edge of each wing was probed to determine the change in amplitude in nanometers (nm) per Pa. This determined at which frequencies the rocking and bending modes occurred. The second study was an angular response at a discrete frequency. This angular response provided the deflection of each wing in nm per Pa as the angle of incidence changed from $-90° \leq \theta \leq 90°$.

The adopted reference system and nomenclature employed for incident angle of sound onto the sensor is shown in Figure 8. The incident angle (θ) is measured as a positive value in the clockwise direction from the normal of the front side of the sensor. The sound source is located in the x-z plane incident upon the x-y plane where the sensor face lies. The left and right wings of the sensor are defined as an observer located at the sensor facing the sound source. For all frequency response plots, the incident direction of sound is at +45° or 45° incidence upon the right wing.

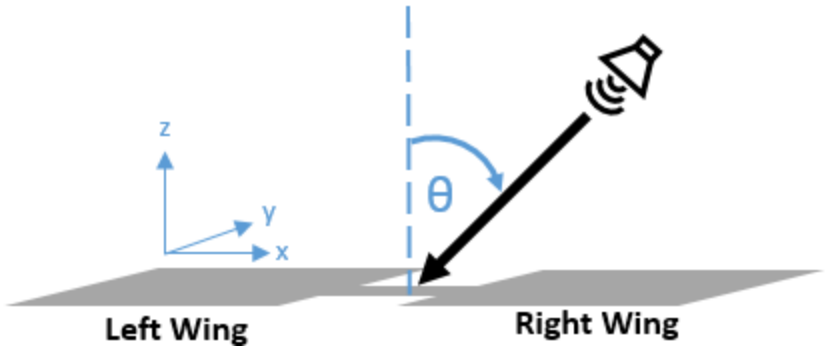

Figure 8. Adopted Reference System and Nomenclature for Incident Angle onto Sensor

A. OPEN BACK SENSOR SIMULATION

The frequency response in terms of amplitude in nm/Pa vs. frequency in Hz for the open back sensor configuration using the COMSOL simulation is shown in Figure 9. The sensor was excited over a frequency range from 1100 Hz to 1800 Hz. The sound was incident at +45º upon the right wing. This configuration shows two resonant peaks at 1340 Hz and 1500 Hz corresponding to the rocking and bending natural oscillation modes, respectively. The amplitude at the rocking frequency is 173 nm/Pa for the left wing and 102 nm/Pa for the right wing (see Figure 9). The amplitude of oscillations at the bending frequency for the left and right wings was found to be nearly the same with a magnitude of 1451 nm/Pa. As expected, the amplitude at the bending mode is an order of magnitude greater than that of the rocking mode. The superposition of the rocking and bending modes at the rocking frequency generated opposing vibration amplitudes as seen in Figure 9.

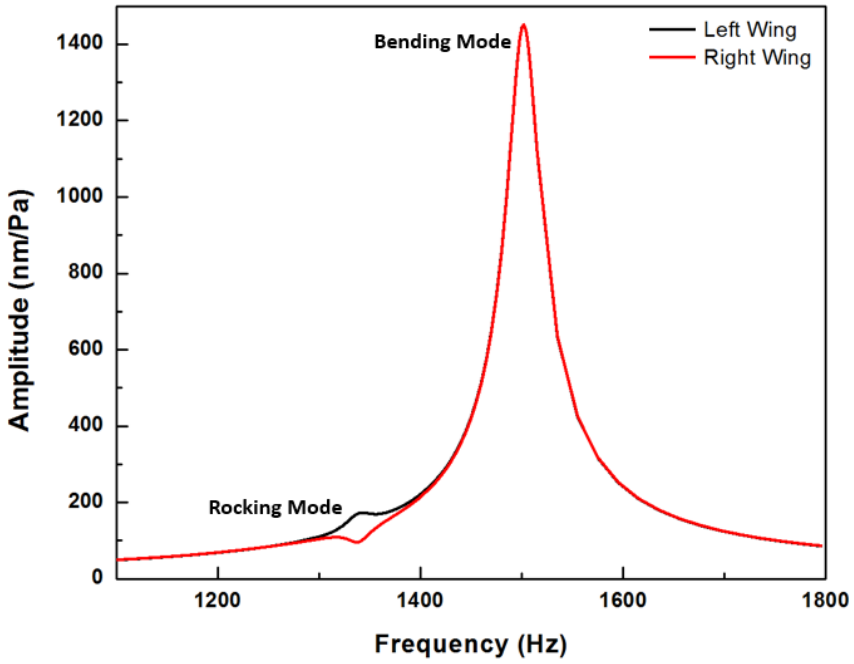

Figure 9. Generation 6–3 Simulated Frequency Response, +45º Incident Angle, Open Back Configuration

The angular response for the open back configuration in terms of amplitude in nm/Pa vs. incident angle was simulated in COMSOL at the rocking mode (1340 Hz) and is shown in Figure 10. When the backside of the sensor is left open, each wing deflects the same amount at two angles of incidence which will result in left and right ambiguity, if the signal from a single wing is used. However, if the difference over sum of the signals from two wings is calculated, the ambiguity can be eliminated as shown in Figure 11. The difference over sum is calculated by

$$\frac{Difference}{Sum} = \frac{A_L - A_R}{A_L + A_R}$$

where A_L is the amplitude of the left wing and A_R is the amplitude of the right wing. More importantly, this equation also removes the sound pressure level which is generally unknown when detecting bearing of a sound source in a real-world application. Figure 11 clearly shows that within the range of $-65° \leq \theta \leq 65°$ there is a distinct difference over sum value for each angle of incidence with a sensitivity of ± 0.35. This simulation shows that within a 130º range of detection, the MEMS direction finding acoustic sensor is able

to discern left and right ambiguity utilizing only one sensor but falls short of the desired 180° range of detection.

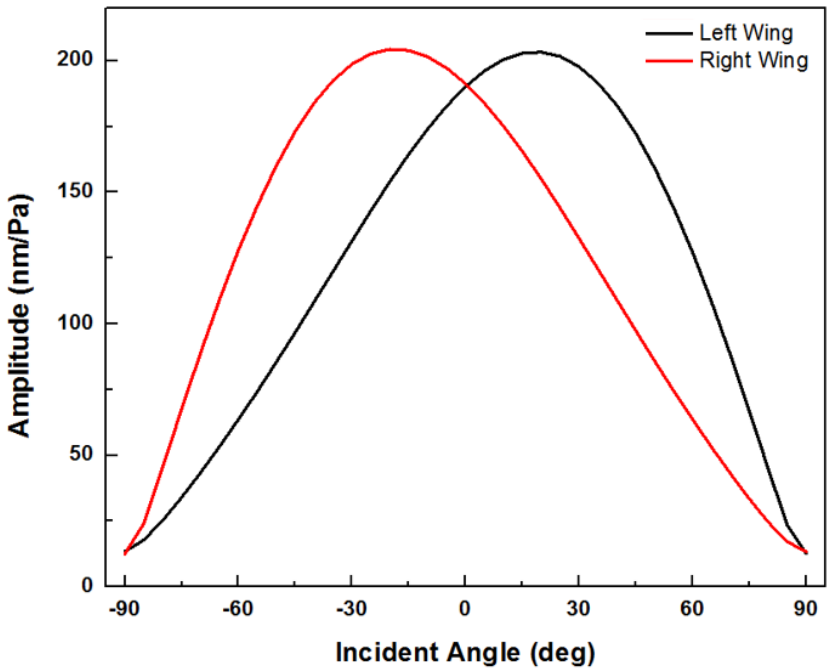

Figure 10. Angular Dependence at 1340 Hz, Open Back Configuration (Gen 6–3 Sensor)

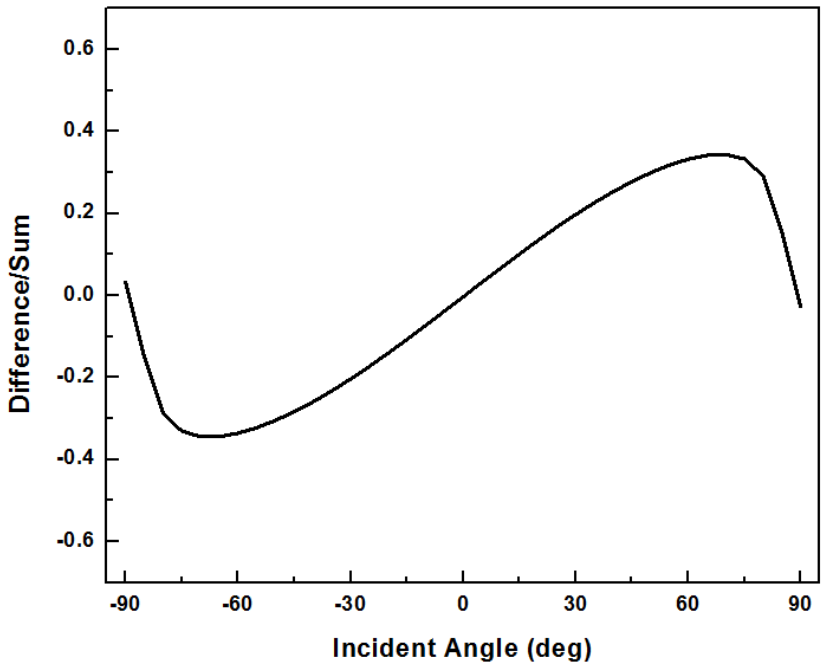

Figure 11. Difference Over Sum Using the Data in Figure 10

B. CLOSED BACK SENSOR SIMULATION

In order to further control the amplitude of both the rocking and bending modes present at a given frequency, it is important to explore the role that the backside air cavity plays. By completely sealing off the backside cavity, there should be little to no coupling of sound from the backside. In addition, the bending mode should be affected by squeezing of the air in the enclosed cavity. The rocking mode should remain unaffected since both wings are moving in opposite directions of one another thereby maintaining the volume of air enclosed behind the sensor without compressing it.

The COMSOL model for the open back sensor configuration was modified by closing the cavity behind the MEMS device attached to the PCB by adding a back plate. The only available air gaps within the simulation are those between the interdigitated comb fingers and the 20 μm trench around the sensor wings and bridge. The frequency response of amplitude in nm/Pa vs. frequency in Hz is shown in Figure 12 and the angular response in nm/Pa vs. incident angle in degrees is shown in Figure 13. With the air cavity behind the sensor fully enclosed, the bending mode is almost entirely suppressed and not visible.

The rocking mode frequency remains the same as the open back configuration at 1340 Hz. The amplitude of the left wing opposite the sound source is greater at 759 nm/Pa than that of the right wing at 473 nm/Pa. Because the bending mode is suppressed, there exists no superposition between the two modes, therefore there is no improvement to the range of angular detection greater than what was already shown in the open back configuration in Figure 11. The difference over sum plot of the closed back configuration is shown in Figure 14.

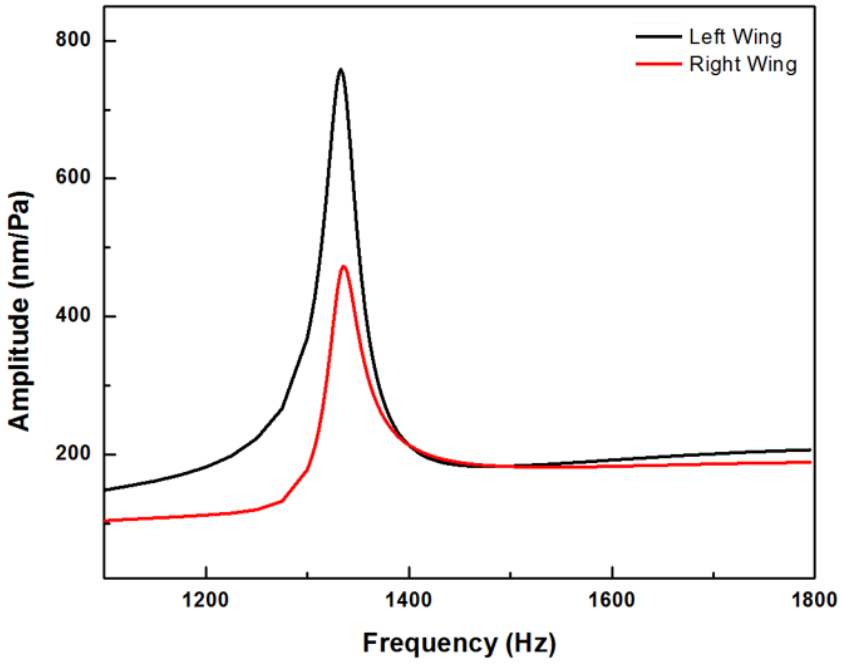

Figure 12. Simulated Frequency Response at +45º Incident Angle with Closed Back Configuration (Gen 6–3 Sensor)

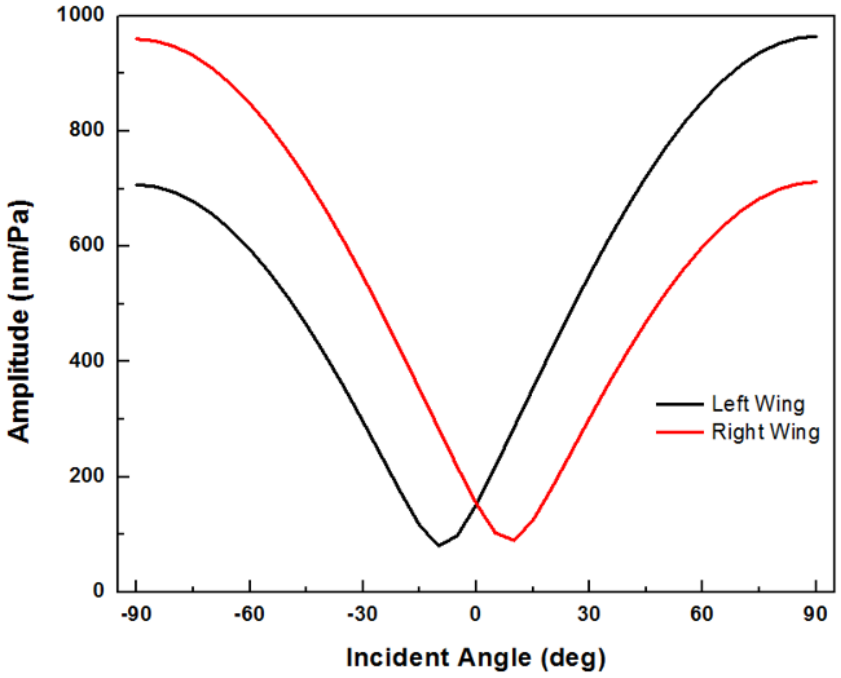

Figure 13. Simulated Angular Response at 1340 Hz, Closed Back Configuration

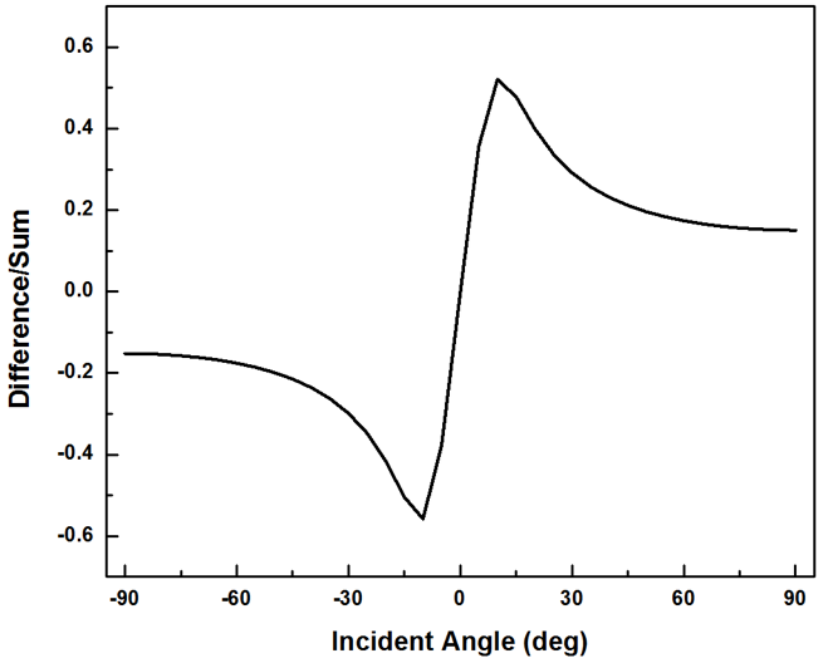

Figure 14. Difference Over Sum at 1340 Hz using the Data in Figure 13

With the absence of the bending mode, the unambiguous determination of incident direction of sound goes down sharply from the open back configuration shown in Figure 11. With the closed back configuration response in Figure 14, it can be seen that the angular span reduces to about 20º from $-10° \leq \theta \leq 10°$, prior to repeating difference over sum values leading to ambiguity. However, the sensitivity has increased from that of the open back configuration to ± 0.6. From this analysis, it can be concluded that completely sealing the backside will not provide us with the ability to detect unambiguous sound over an entire 180º range. The solution needs to contain the rocking mode as well as the bending mode but cannot be dominated by one or the other.

C. SIMULATION WITH HOLE IN BACK PLATE

In order to optimize the amplitude of the bending mode without suppressing it completely, a hole is created at the center of the back plate. By varying the size of the hole, the damping and coupling of sound from the backside can be controlled for enhancing the amplitude at that bending frequency. In order to determine the appropriate size of the hole, a parametric sweep of frequency responses was performed over a range of hole radii. A 1.2 mm radius hole in the back plate demonstrated a response that brought the amplitude of the bending mode down to roughly the same size as the rocking mode while still keeping the two modes separated. If the hole is too small, the frequency response approaches that of the closed back configuration and if the hole is too large, the frequency response approaches that of the open back configuration. The simulated frequency response of the 1.2 mm hole is shown in Figure 15. In the simulation, the rocking mode occurs at 1325 Hz and the bending mode at 1400 Hz. The frequency separation between the two modes has reduced compared to that of the open back configuration in Figure 9. Whereas before the frequency separation was 160 Hz, now the separation between modes is only 75 Hz. The shift of the bending resonance frequency to a lower value indicates damping generated when the air in the cavity squeezes through the hole.

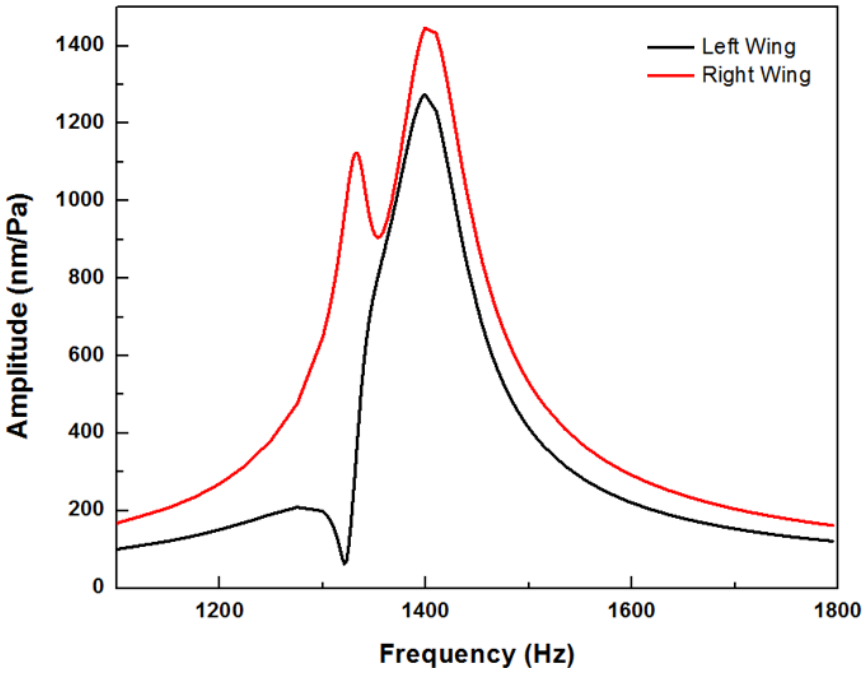

Figure 15. Simulated Frequency Response at +45º Incident Angle, 1.2 mm Radius Hole in Back Plate (Gen 6–3 Sensor)

An angular response was simulated on the sensor with a 1.2 mm hole at 1330 Hz and the results are shown in Figure 16. Again, the difference over sum was taken to see the range of unambiguous incident angle detection and it can be seen that the overall range has degraded from that of the open back configuration as shown in Figure 17. With an optimally determined size hole in the back plate, the greatest angular detection range obtained is from $-45° \leq \theta \leq 45°$ with a sensitivity of ± 0.6. This range of 90º is far less than that of the previously simulated 130º from the open back configuration.

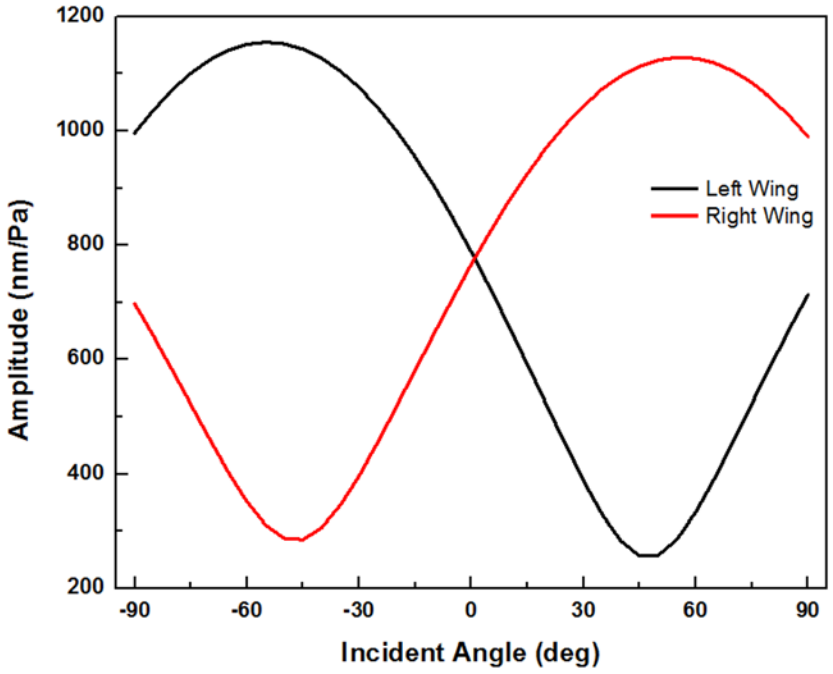

Figure 16. Simulated Angular Response at 1330 Hz with 1.2 mm Radius Hole in Back Plate

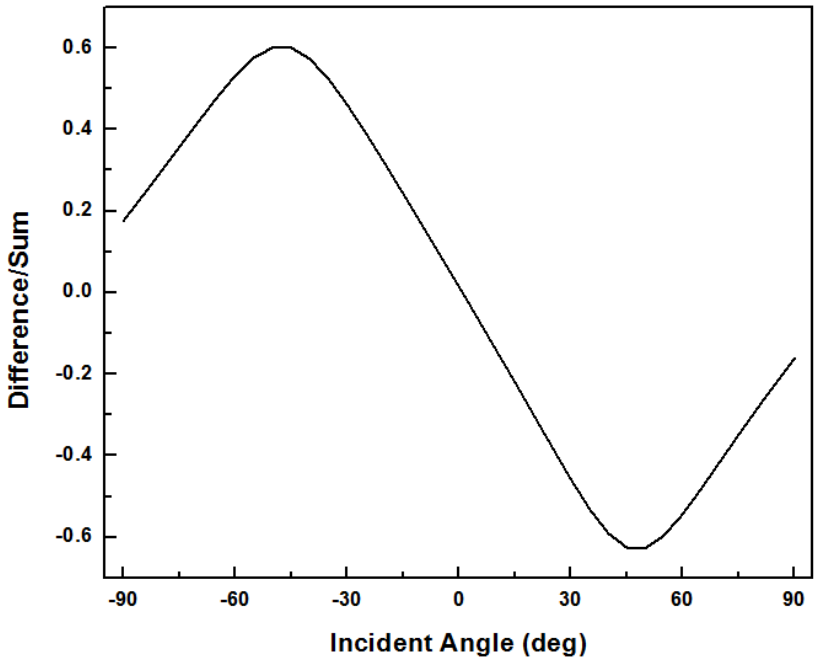

Figure 17. Difference Over Sum at 1330 Hz Using the Data in Figure 16

This simulation with a back plate hole shows the limitations in the design of the Generation 6–3 sensor, which was not optimized for this mode of operation. Although the back plate hole was successful in controlling the superposition between the two modes it was not successful in extending the range of angular detection greater than 130º. This is presumably due to the limited difference in frequency between the two natural oscillation modes once the air cavity in the backside is constrained with the use of a small hole. Just as the superposition of the two modes breaks down if they occur at frequencies too distant from one another, if the modes are too close together the ability to discern incidence angle is degraded. In order to solve this problem, a new sensor will have to be designed with geometry that supports an appropriate frequency separation between the rocking and bending modes.

THIS PAGE INTENTIONALLY LEFT BLANK

III. EXPERIMENTAL SETUP AND RESULTS

For the measurement of sensor characteristics, the sensor is integrated with readout electronics. A cross sectional schematic of the MEMS directional acoustic sensor attached to the readout electronics circuit board is shown in Figure 18. The sensor (A) was glued onto a 2.5 mm thick PCB (B) over a hole that was milled through the entirety of the board. The hole had a 1 mm wide lip around the edge to place the sensor. The adhesive (C) was ultraviolet (UV) curing Norland Optical Adhesive 68 which allowed for a low stress bonding of the sensor die to the PCB. Previous adhesives such as two-part epoxy exhibited too rigid of a bond between the sensor and the PCB which affected the sensor performance due to residual stress between the sensor and circuit board. The transfer of stress through the adhesive to the sensor was minimized with the UV glue.

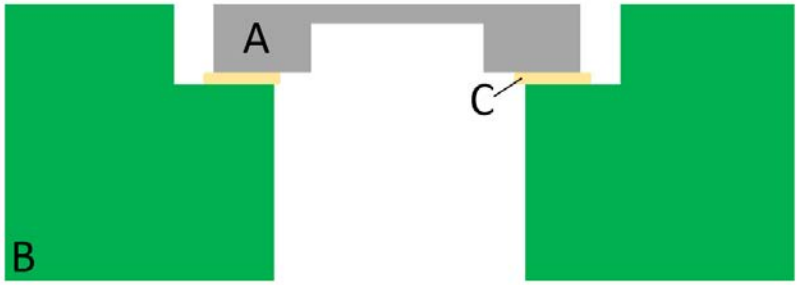

Figure 18. Cross Sectional Schematic View of Open Back Sensor (A) on PCB (B) with UV Glue (C). Adapted from [14].

In order to control the amplitude of the bending mode of the sensor, a closed back attachment was designed and utilized. The finite air cavity behind a closed back sensor provides a restoring force to the wings during the bending mode of oscillation. Theoretically, if the backside of the sensor was a perfectly sealed cavity, the bending mode of oscillation would nearly disappear as the restoring force against the wings would be too strong. In reality, the air gaps between the capacitive comb fingers as well as the gap around the sensor provides some air flow allowing a damped bending mode. In order to accurately control the damping force that the air cavity enacts on the sensor a hole was milled into the back plate. The hole (D) was milled into a separate piece of blank PCB and UV glued (C)

to the backside of the main circuit board (B) as shown in Figure 19. The completed sensor assemblies for the open and closed back configurations mounted on a 3-D printed housings are shown in Figure 20.

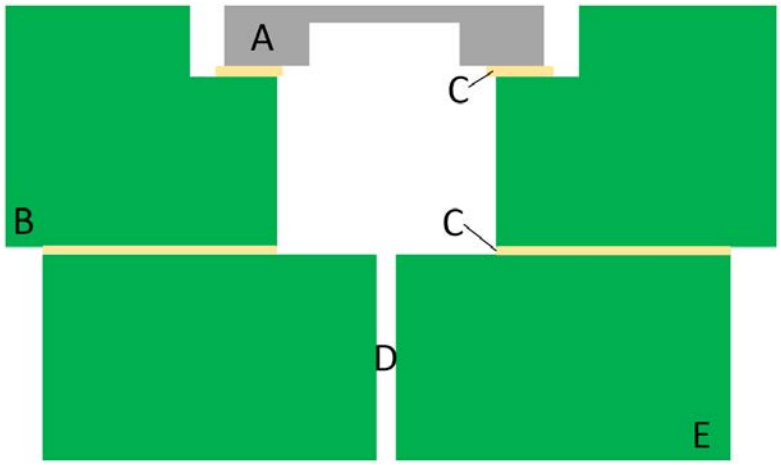

Figure 19. Cross Sectional Schematic View of Closed Back Sensor with Backside Hole (D) on PCB with UV Glue. Adapted from [14].

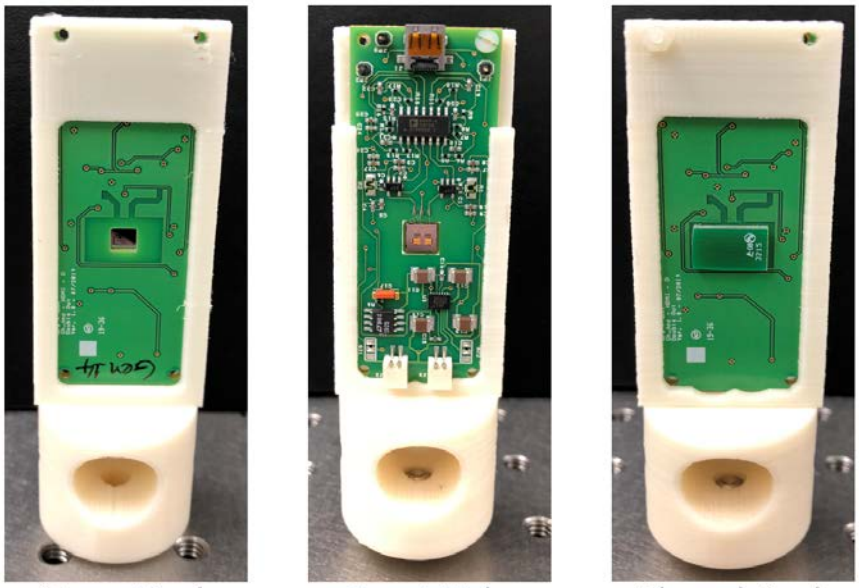

Figure 20. Images of the Completed Sensor Assemblies for Two Configurations Attached to 3-D Printed Housings

In order to measure both the frequency and angular responses, the sensor mounted on the circuit board was attached to a Brüel and Kjær controllable turntable type 5960 within the anechoic chamber as shown schematically in Figure 21. The sensor was connected via an HDMI cable to both the Agilent DC power supply model E3620A and the two MFLI Lock-In Amplifiers (500 kHz/5 MHz, 60 MSamples/s) by means of a breakout board. Specifically, the signal from each wing went to an individual MFLI that were synchronized and controlled by the Zurich Instruments LabOne software. This allowed for measurement of signals from each wing when excited by the sound source. The sound source was a fixed loudspeaker directed at the turntable that was excited using the LabOne software via a Techron Power amplifier model 5507. When conducting the frequency response of the sensor, the turntable was kept at a fixed angle of incidence with respect to the sound source while the frequency of sound source swept over a specified range. For the angular response, the sound source was excited at a fixed frequency while the turntable was rotated at a constant speed. A PCB Piezotronics omnidirectional microphone model 378A21 was placed in the vicinity of the sensor in the same orientation towards the speaker at the start of every measurement in order to capture the sound pressure level and normalize the measured signals from the MFLI Lock-In Amplifier from Volts (V) to V/Pa.

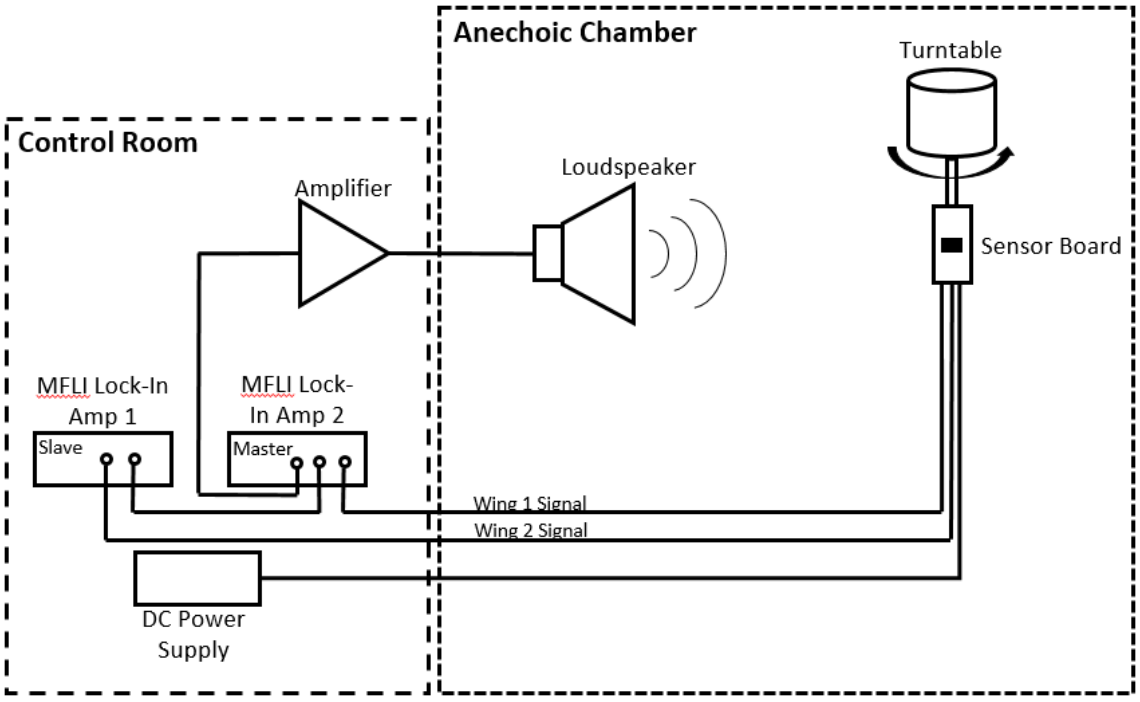

Figure 21. Block Diagram for Frequency and Directional Measurements Inside an Anechoic Chamber

A. OPEN BACK SENSOR RESPONSE

The measured frequency response for the open back sensor in the anechoic chamber is shown in Figure 22. The sensor was excited over a frequency range from 1100 Hz to 1800 Hz at a sound source voltage amplitude of 9.99 mV_{pk}. The sound was incident at +45º upon the right wing. The measurement shows two resonant peaks at 1254 Hz and 1460 Hz corresponding to the rocking and bending natural oscillation modes, respectively. The amplitude at the rocking frequency is 1.01 V/Pa for the left wing and 2.74 V/Pa for the right wing. The amplitude for the bending frequency for the left wing is 18.12 V/Pa and 18.87 V/Pa for the right wing. As demonstrated in the COMSOL simulations of the open back configuration, the bending mode amplitude is roughly an order of magnitude greater than the rocking mode amplitude.

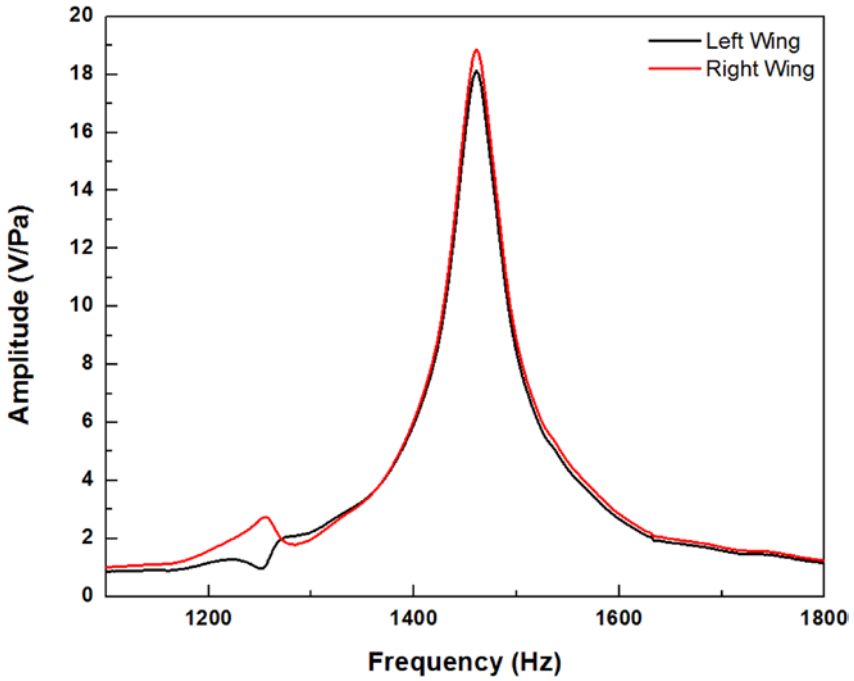

Figure 22. Measured Frequency Response at +45º for Open Back Configuration (Gen 6–3 Sensor)

In order to compare the results of Figure 22 to those of the COMSOL simulations in Figure 9, amplitudes of both data sets were normalized from 0 to 1 and then plotted together as shown in Figure 23. It can be seen that responses between the FE simulations and experimental data are similar except the FE simulation rocking and bending peaks shifted to higher frequencies. The larger shift associated with the rocking mode can be attributed to the fixing of the torsional leg at the substrate in the COMSOL model which may not be true. In reality, the undercut of substrate where the legs connect to the substrate during the SOIMUMPs process could make the connection from the legs to the substrate less rigid making the resonant frequency lower. In addition, the nominal device layer thickness of 25 µm used in the simulation can vary by 1 µm as indicated in the SOIMUMPs Handbook [6]. These effects ultimately can cause the rocking and bending modes to occur at lower frequencies.

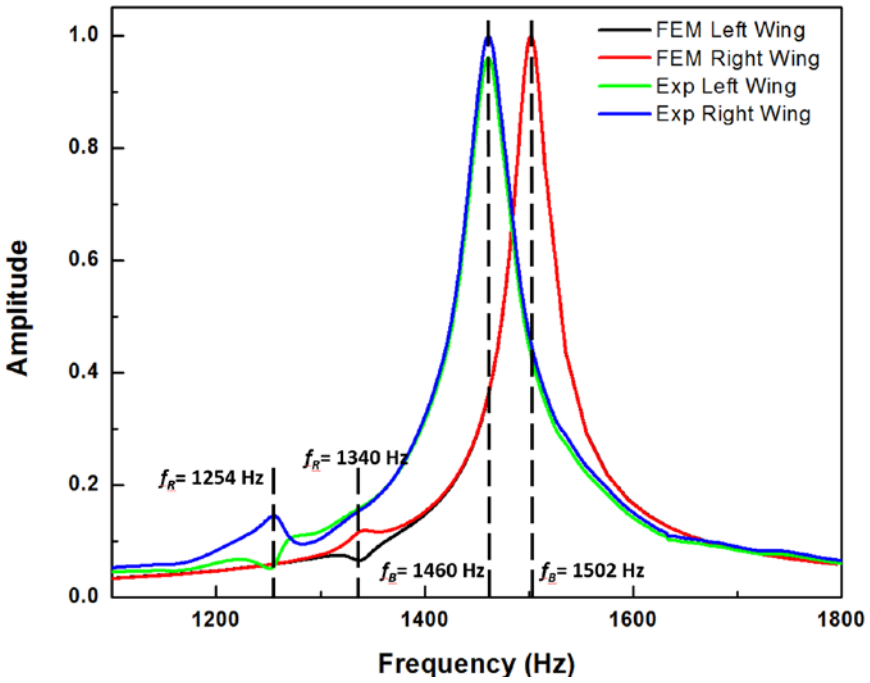

Figure 23. Comparison of Frequency Responses Between Simulated and Experimental at +45º Incident Angle for Open Back Configuration (Gen 6–3 Sensor)

The angular response for the open back configuration was measured at the rocking mode (1254 Hz) and is shown in Figure 24. When the backside of the sensor is left open, it can be seen that each wing deflects the same amount at two different angles of incidence which will result in left and right ambiguity if the signal from a single wing is used. For example, if the deflection of the right wing was measured at 2 V/Pa, there would be no way to discern whether the incident angle was -30º or 60º. The difference over sum of the two wings is calculated at 1254 Hz and is shown in Figure 25 which shows that within the range of $-65° \leq \theta \leq 65°$ there is a distinct difference over sum value for each angle of incidence with a sensitivity of ± 0.4. This shows that within a 130º range of detection, the MEMS direction finding acoustic sensor is able to discern left and right ambiguity utilizing only one sensor. As with the simulated response, the open back configuration falls short of the desired 180° angular detection range.

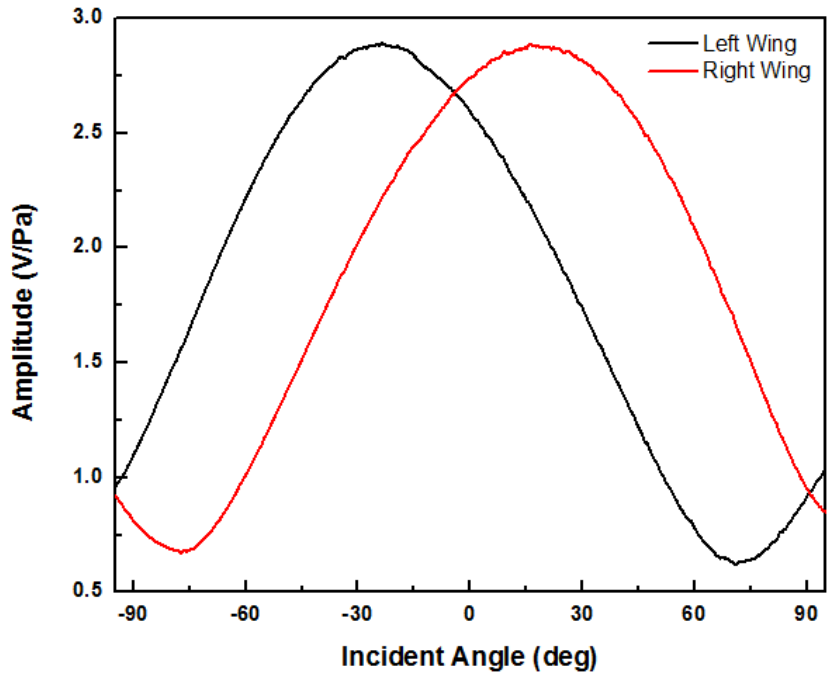

Figure 24. Angular Response at 1254 Hz for Open Back Configuration (Gen 6–3 Sensor)

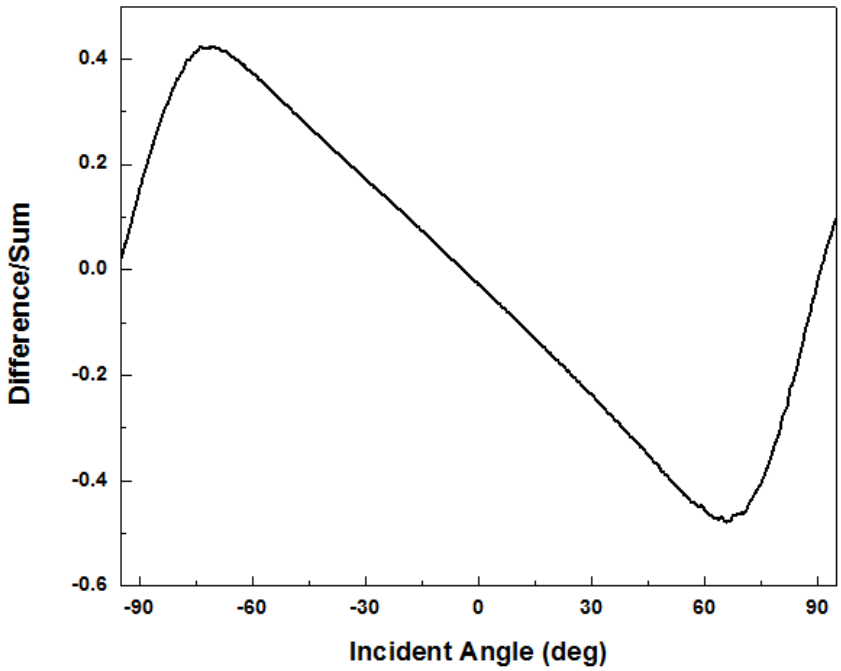

Figure 25. Difference Over Sum Using the Data in Figure 24

B. CLOSED BACK SENSOR RESPONSE

To create the closed back configuration as depicted in Figure 20, the back of the circuit board was hermetically sealed with a blank piece of PCB with UV curing adhesive. The sensor assembly was then tested in an identical manner to the open back configuration in the anechoic chamber. The frequency response of the closed back sensor in V/Pa vs. frequency in Hz is shown in Figure 26. The sound was incident at +45°.

The measured frequency response shows a nearly identical behavior as that of the simulation with the closed back configuration. Figure 27 shows a comparison between the measured and simulated data. The sensor exhibited a rocking mode at 1254 Hz. This is compared to the COMSOL simulation that showed a rocking mode occurring at 1340 Hz as expected. The bending mode has been almost completely damped by sealing off the cavity behind the sensor. The differences in amplitude of the right wing at the rocking frequency between the simulated and measured response in Figure 27 can be attributed to the deviations in geometry of the manufactured sensor due to tolerances in the SOIMUMPs process versus a COMSOL model with perfect geometry.

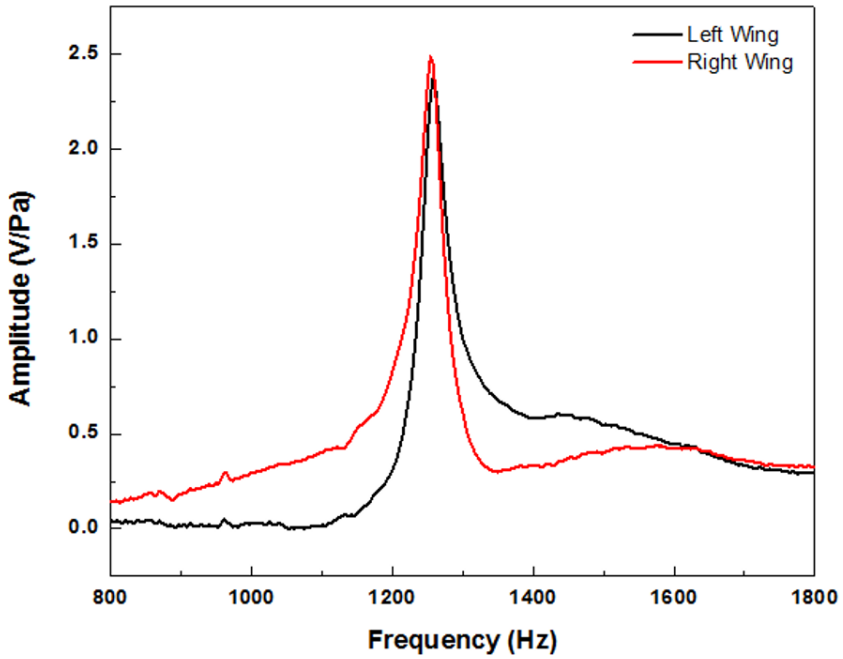

Figure 26. Frequency Response at +45º Incident Angle with Closed Back Configuration (Gen 6–3 Sensor)

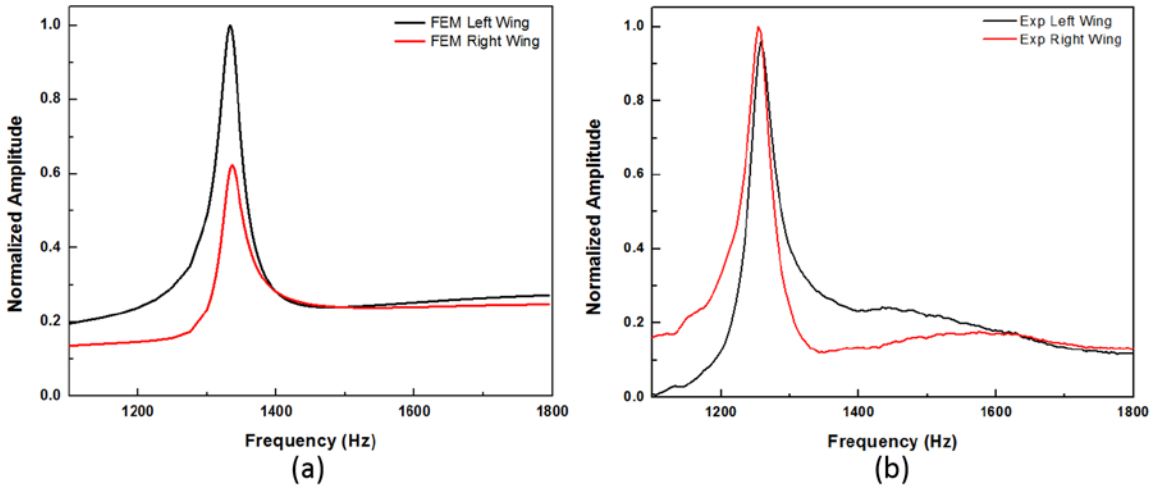

Figure 27. Comparison of Frequency Responses Between (a) COMSOL Simulation and (b) Experimental at +45º Incident Angle with Closed Back Configuration (Gen 6–3 Sensor)

The measured angular response of the backside closed configuration at the rocking mode of 1254 Hz is shown in Figure 28(a) and the corresponding difference over sum plot is shown in Figure 28 (b). As predicted from the COMSOL simulation in Figures 13 and 14, the directional response of the Generation 6–3 sensor with a closed back is found to be poor. The bending mode is nearly completely damped away, leaving only the directional response from the rocking mode. Because of this, the usable angular detection range has been reduced to a very narrow range from about $-10° \leq \theta \leq 0°$.

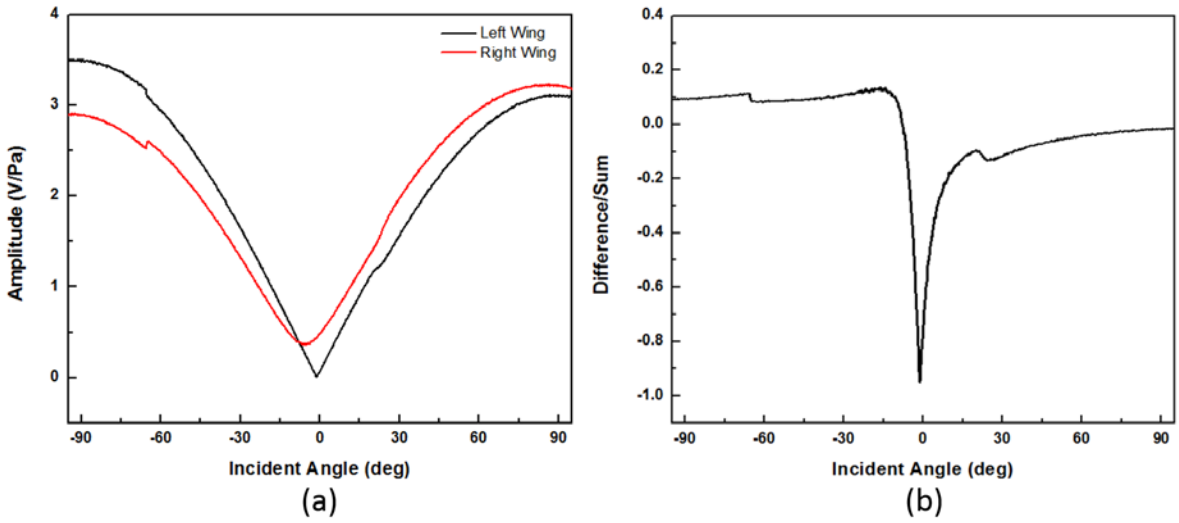

Figure 28. (a) Angular Response at 1254 Hz for Closed Back Configuration and the (b) Difference Over Sum Using the Data in Figure 28(a)

C. SENSOR RESPONSE WITH HOLE IN BACK PLATE

For measuring the sensor response in this configuration, the PCB blank used for closing the back was removed and a 750 µm radius hole was milled through in the center. The PCB piece was then glued on the circuit board behind the sound sensor with UV curing adhesive. The sensor was then tested in an identical manner to the closed back configuration in the anechoic chamber.

The measured frequency response in V/Pa vs. frequency in Hz is shown in Figure 29. It can be seen that the rocking mode occurs at 1254 Hz and the responses of the two wings have a wide difference in amplitude while the damped bending mode at 1400 Hz shows both wings exhibit nearly the same amplitude. In addition, the peak position of the bending mode shifted to a lower value with an increased FWHM compared to that observed in open back configuration. This behavior is expected as the air in the cavity gets squeezed and escapes through the hole, the damping is increased which can lower the peak position with a higher bandwidth. The simulation of the sensor frequency characteristics with the back hole shown in Figure 30 (a) agrees well with the measurements in Figure 29.

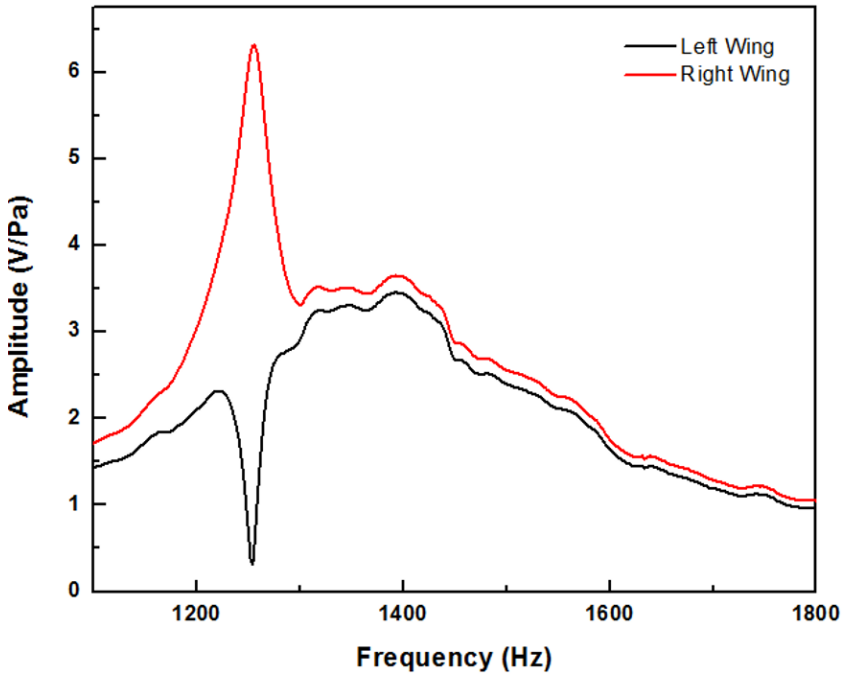

Figure 29. Frequency Response at +45° Incident Angle, 750 µm Radius Hole in Back Plate. (Gen 6–3 Sensor)

A comparison of both the FE simulation data from COMSOL and the experimental data from the anechoic chamber in the back plate hole configuration is shown in Figure 30(a) and (b), respectively. Both data sets have normalized amplitudes to allow for easier comparison between the two plots. It is important to note that for the FE data, the hole in the back plate had a radius of 1200 µm whereas the experimental data is from a hole with radius of 750 µm in the back plate. The experimental hole was driven by available resources of milling bits in the sensor research lab. The COMSOL model was parameterized to find the closest hole size that shows a similar response to that found experimentally, which resulted in a 1200 µm simulated radius. To expect a perfect match between the two radii would assume no differences in dimension on the micro scale which is not feasible. The differences between the two radii most likely stem from the variations in tolerance when the sound sensor is etched during the SOIMUMPs process. During the manufacturing of the completed board assembly, the sensor may not be perfectly hermetically sealed to the PCB nor the back plate be perfectly sealed to the PCB. Both of

these imperfections would cause a change to the available air cavity that is damping the backside of the sensor.

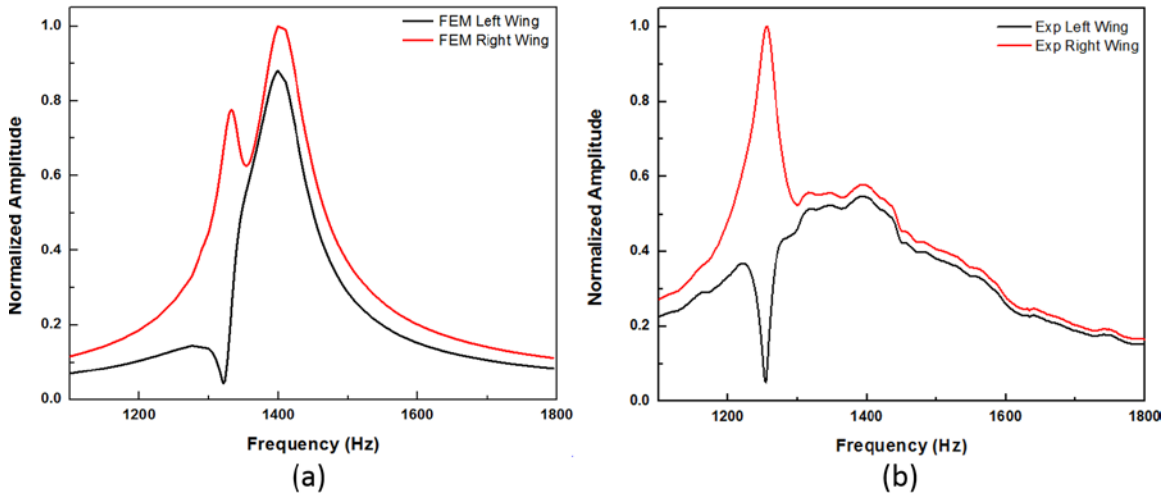

Figure 30. Comparison of Frequency Responses at +45° Incident Angle, (a) COMSOL Simulation with 1200 µm Radius Hole, (b) Measurement with 750 µm Radius Hole (Gen 6–3 Sensor)

The angular response for the sensor with a 750 µm radius hole in the back plate was measured at 1254 Hz and the results are shown in Figure 31(a). The corresponding difference over sum plot is shown in Figure 31(b) and it can be readily seen that there is an improvement in the angular detection from the backside closed configuration of the sensor, with a range of $-45° \leq \theta \leq 45°$. The bending mode is slightly more prominent resulting in broader angular detection range due to the superposition of the two modes. When compared to the open back configuration shown in Figure 25, the overall detection range has decreased from 130° to 90° but the sensitivity (maximum to minimum of difference over sum) has nearly doubled.

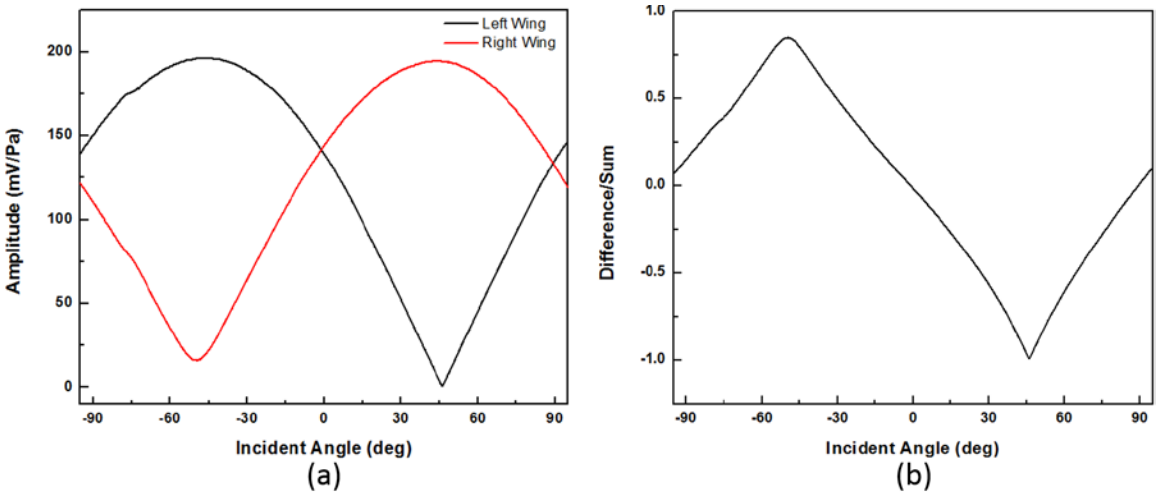

Figure 31. (a) Angular Response at 1254 Hz with 750 µm Radius Hole in Back Plate and (b) Difference Over Sum Using the Data in Figure 31 (a)

For the simulations shown in Chapter II, a detectable angular range of 90° was achieved with a hole in the back plate. When testing the sensor in the anechoic chamber, a nearly identical response was measured with a detectable range of 90°. The comparison between simulated and experimental data shows that the COMSOL model provides an accurate representation of the actual response and characteristics shown by the sensor. Therefore, COMSOL can be used to determine an optimum geometry of a new generation of sensor with the effect of creating a full 180° range of angular detection.

THIS PAGE INTENTIONALLY LEFT BLANK

IV. OPTIMIZATION OF SENSOR GEOMETRY

Based on the initial experimental observations, the existing COMSOL models were refined to design a sensor that can provide 180° angular coverage. A schematic of an optimized sensor is shown in Figure 32. The sensor consists of two wings that are 1200 µm by 1600 µm in area which are connected to each other via a 2700 µm long and 30 µm wide bridge. The wings are smaller in surface area by about 42% than the Generation 6–3 sensor used in the previous measurements. Perpendicular to the center of the bridge are two 400 µm long and 40 µm wide torsional legs that connect the bridge and to the substrate. By making the torsional legs thinner, less toque will be required to pivot the wings during the rocking mode therefore shifting the rocking mode frequency down compared to that of the Generation 6–3 sensor. The comb fingers are organized into a fishbone pattern [12] that enhances the structural stability as shown in Figure 33. There is a 2 µm gap between each of the comb fingers. The entire structure of the sensor with the exception of the two points where the torsional legs attach to the substrate is surrounded by a 10 µm gap between the moving portion of the sensor and the rest of the substrate. The dimensions of the sensor are shown in Figure 32. The modifications to the geometry increase the frequency gap between the rocking and bending modes to achieve better superposition of the two modes and therefore the directional response of the sensor.

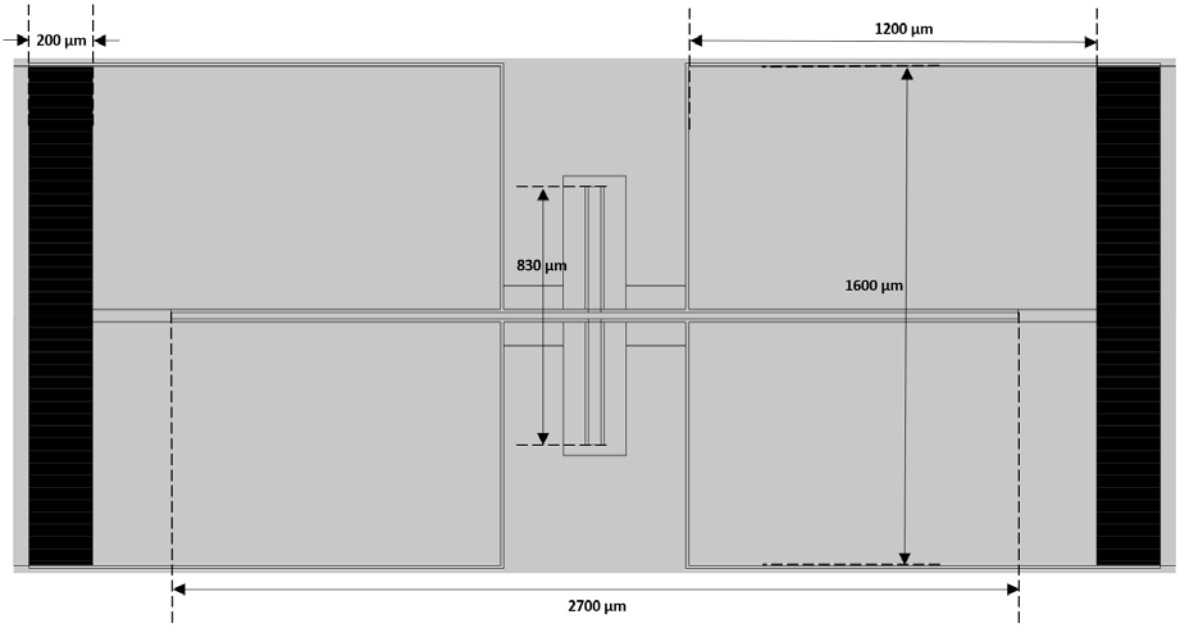

Figure 32. COMSOL Model of Sensor with Major Dimensions

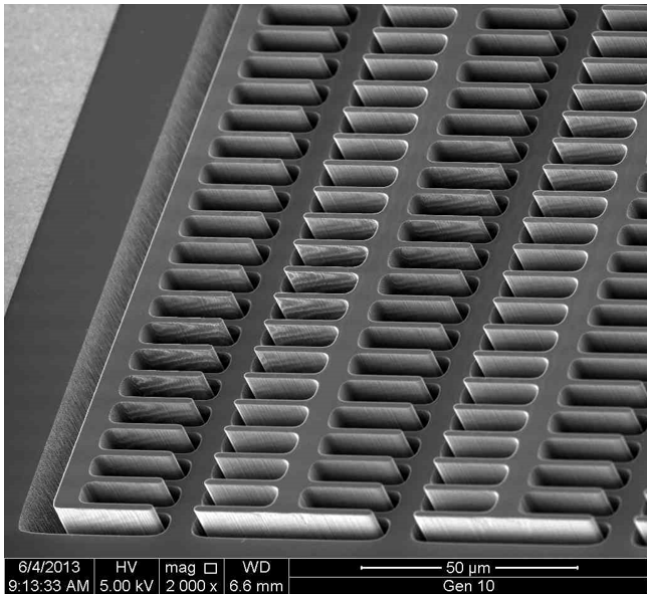

Figure 33. SEM Image of Interdigitated Comb Fingers Source: [12].

The simulation of sensor characteristics we carried out as before using COMSOL employing the solid mechanics, pressure acoustics, and thermoviscous acoustics physics. A plane wave with 1 Pa amplitude was incident upon the sensor. The sensor was modeled in the open back, closed back, and with a hole in the back plate configurations. The

frequency response was performed on the sensor over a range of frequencies to analyze the deflection in nm/Pa of each wing in order to determine the rocking and bending frequency modes. The incident angle of sound was kept at +45° for all the configurations. The second study performed was angular response at a discrete frequency where the incident sound source was swept across the sensor over 180° to determine the deflection of each wing in nm/Pa. The angular data was converted to a difference over sum plot to analyze the directional sensitivity of the sensor in each configuration as well as to determine the range of unambiguous angular detection.

A. OPEN BACK SENSOR SIMULATION

The sensor frequency response was analyzed in COMSOL and the amplitude in nm/Pa vs. frequency in Hz for the open back sensor configuration is shown in Figure 34. This configuration shows two resonant peaks at 1140 Hz and 1525 Hz corresponding to the rocking and bending natural oscillation modes, respectively (see Figure 34). The angular response is shown in Figure 34 for a frequency that fell between the rocking and bending modes and showed the greatest difference between the left and right amplitudes (or sensitivity) in that angular range. The difference over sum was then plotted in Figure 36 which shows that the open back configuration of the sensor has an unambiguous detection range of $-75° \leq \theta \leq 75°$ or 150° overall with relatively low sensitivity of ± 0.35.

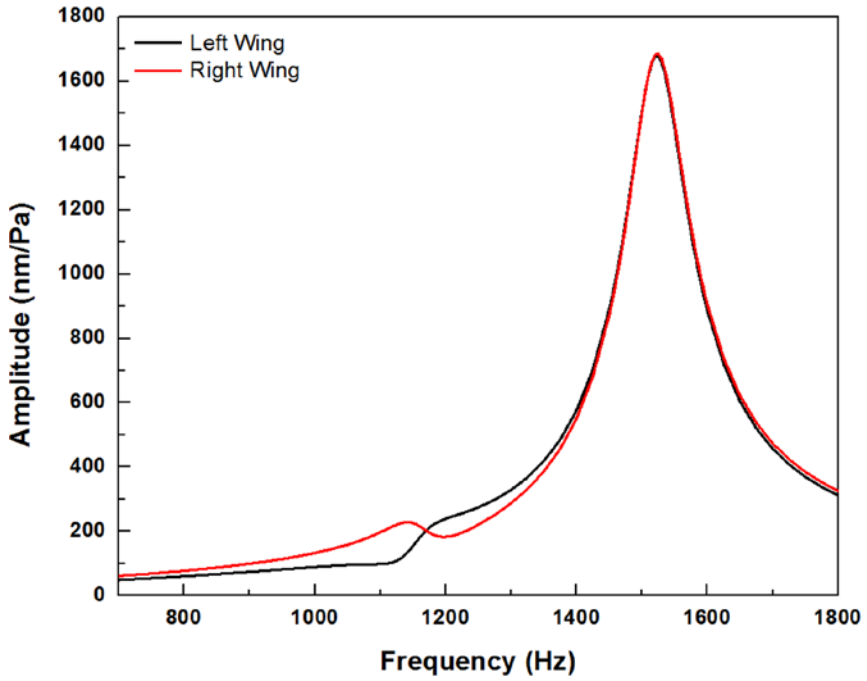

Figure 34. Simulated Frequency Response at +45 Incident Angle with Open Back Configuration

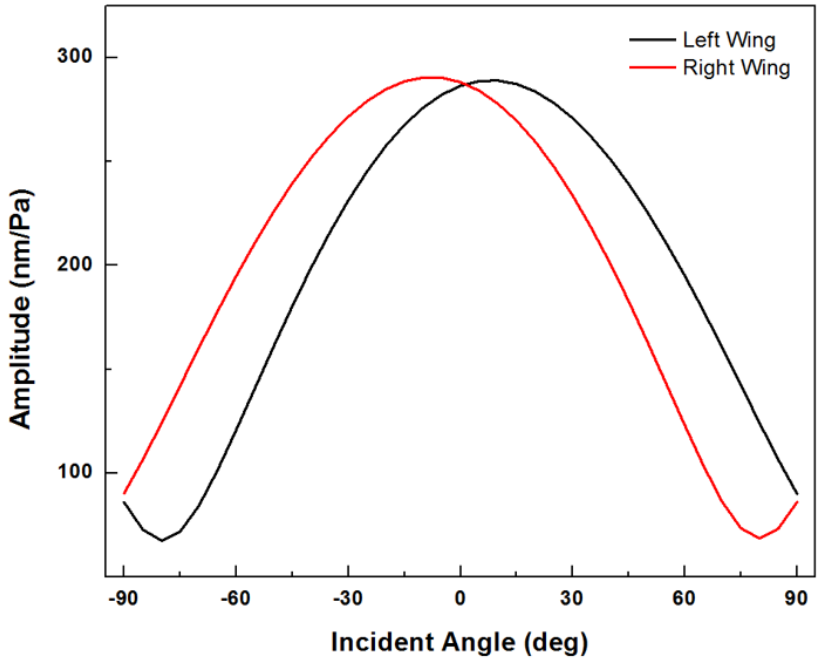

Figure 35. Angular Dependence at 1200 Hz with Open Back Configuration

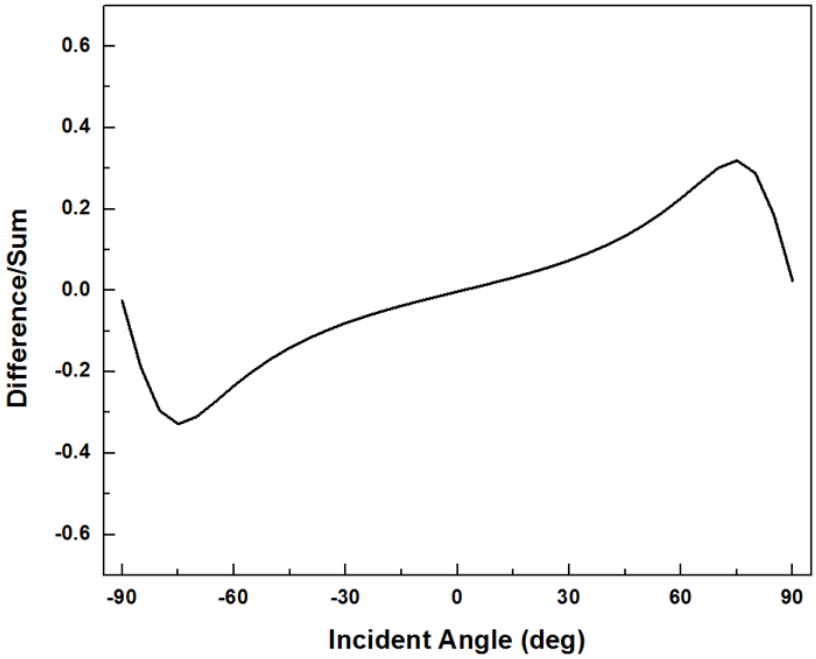

Figure 36. Difference Over Sum Using the Simulated Data in Figure 35

B. CLOSED BACK SENSOR SIMULATION

The same modifications were made to the sensor model as the Generation 6–3 to convert it from the open back configuration to the closed back configuration. The only available air gaps were now the 10 µm trench around the movable portions of the sensor and the 2 µm gaps around the fishbone comb fingers. The frequency response for the closed back configuration in terms of amplitude in nm/Pa vs. frequency in Hz is shown in Figure 37. The rocking frequency remains relatively unchanged at 1150 Hz but the bending mode has shifted to a much higher frequency of 2150 Hz. By closing the backside, we hypothesized that the bending mode would be completely damped, as it had been in the Generation 6–3 sensor. However, it can be seen in Figure 37 that the bending mode for the closed back configuration is still present at a higher frequency and additional modes are present over 3000 Hz (see Figure 37). These additional modes showed little directional sensitivity and were not analyzed in this research. The shifting of the bending mode to a higher frequency can be attributed to the stiffness of the air volume trapped in the cavity behind the wings which gets compressed due to in phase motion of the wings. The rocking

mode is not affected by it since the wings are moving in out of phase keeping the air volume the same.

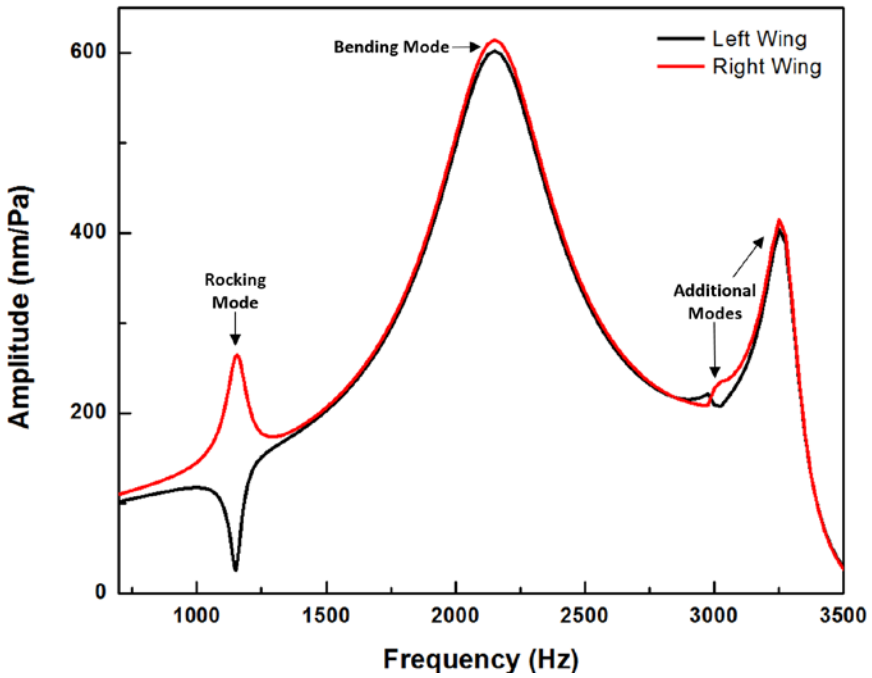

Figure 37. Simulated Frequency Response at +45º Incident Angle with Closed Back Configuration

The angular response in terms of amplitude in nm/Pa vs. incident angle in degrees at the rocking mode of 1150 Hz is shown in Figure 38 with the subsequent difference over sum plot in Figure 39. The optimized geometry of the sensor shows improvements in sensitivity is ± 0.95 as well as the range of $-60° \leq \theta \leq 60°$. The highest sensitivity observed with the closed back Generation 6–3 sensor was only ± 0.6 over a much narrower angular range ($-10° \leq \theta \leq 10°$) as shown in Figure 14. As observed with the Generation 6–3 sensor, it is expected that by adding a hole in the back plate, it will be able to control the superposition of the two modes and increase the unambiguous detection range of the sensor to 180°.

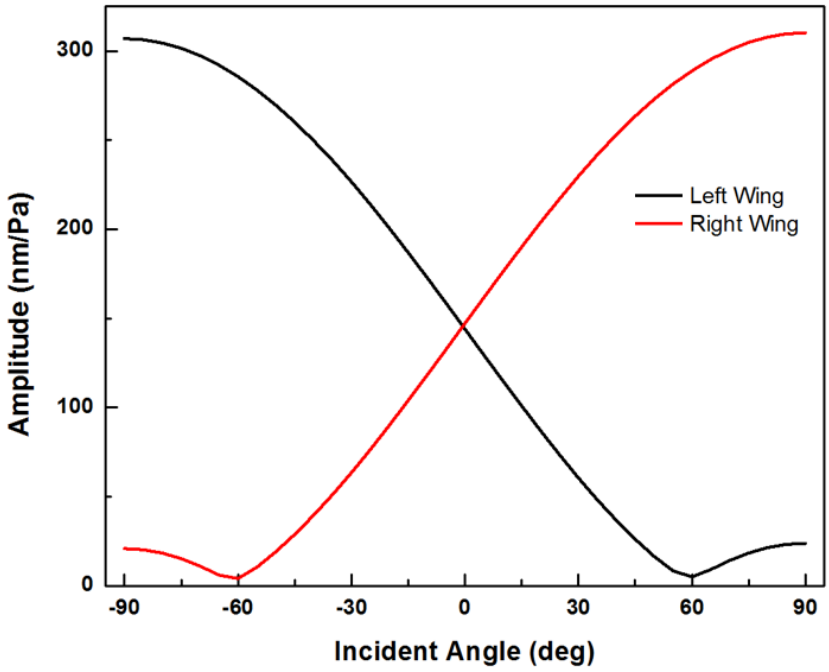

Figure 38. Angular Dependence at 1150 Hz with Closed Back Configuration

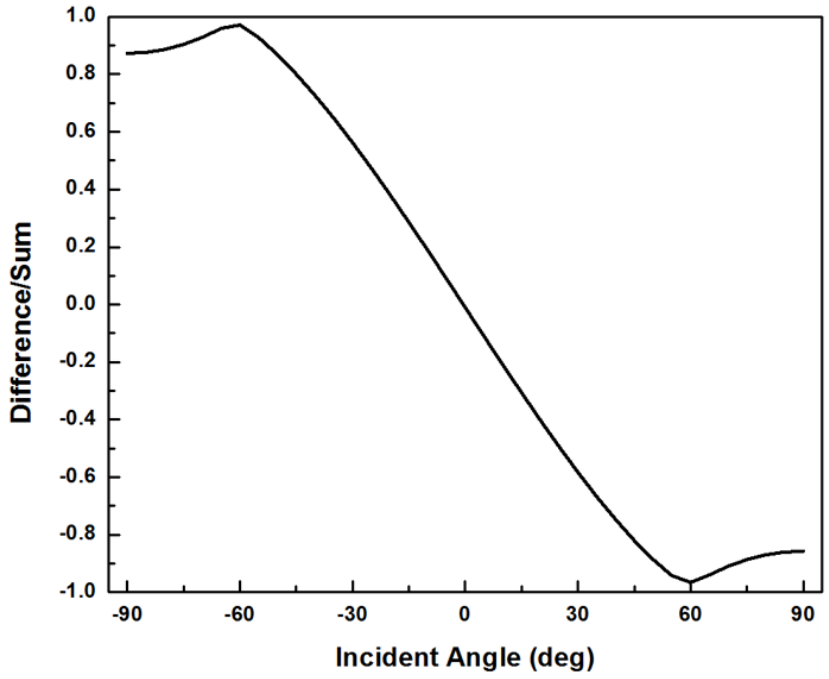

Figure 39. Difference Over Sum Using the Simulated Data in Figure 38

C. SIMULATION WITH HOLE IN BACK PLATE

The model the new sensor was modified by adding a hole in the back plate of the enclosed air cavity. In order to determine the appropriate size of the hole, a parametric sweep of frequency responses was performed over a range of hole radii. At hole radii less than 200 µm, an additional bending-like mode was present that occurred at a lower frequency than the rocking mode, shown as the First Bending Mode in Figure 40. After again parameterizing hole radii less than 200 µm and studying their effects on directionality, a 150 µm radius hole was chosen and analyzed. The first bending mode occurs at 750 Hz and has roughly the same amplitude as the rocking mode (see Figure 41). By analyzing the stress felt by the sensor in COMSOL at that frequency, we can see that both wings are deflecting in the same direction just as we have seen with the original bending oscillation mode. All other modes remained unchanged from the closed back configuration.

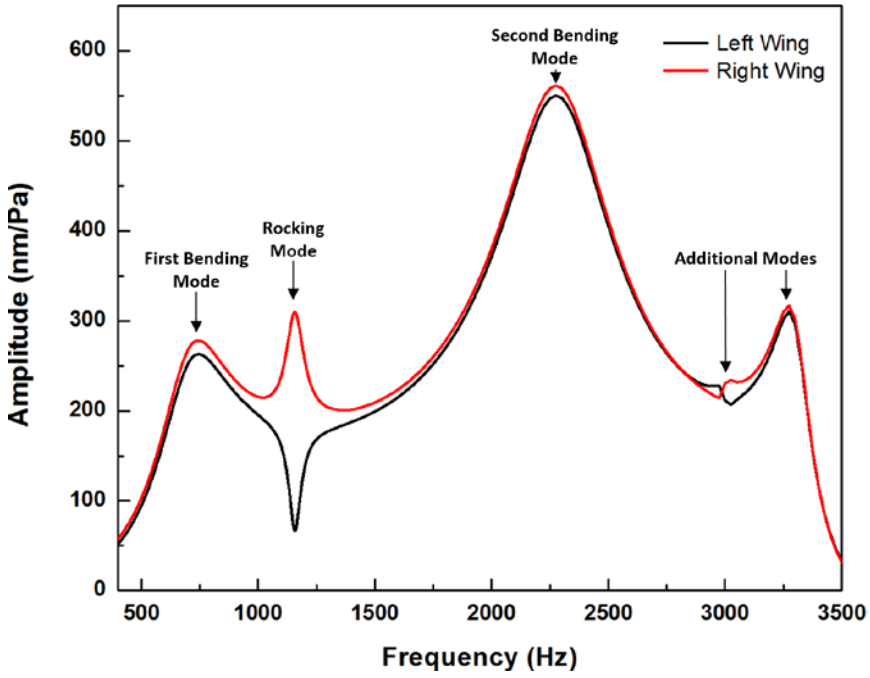

Figure 40. Simulated Frequency Response at +45° Incident Angle with a150 µm Radius Hole in Back Plate

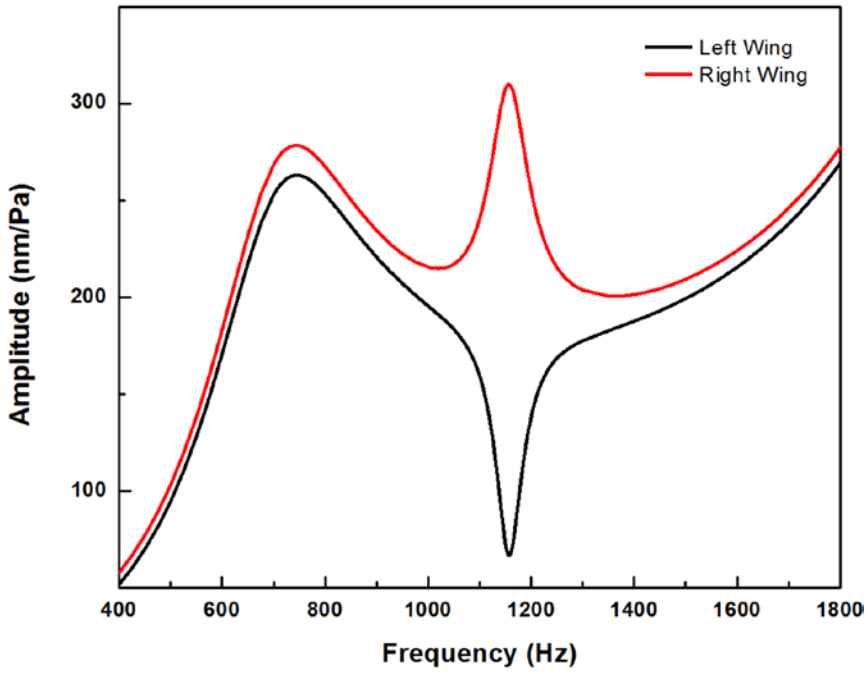

Figure 41. Simulated Frequency Response at +45º Incident Angle with a 150 µm Radius Hole in Back Plate

The angular response in terms of amplitude in nm/Pa vs. incident angle at the rocking mode of 1140 Hz is shown in Figure 42 and the difference over sum is shown in Figure 43. From the angular dependence in Figure 42 it can be seen that each wing has a distinct amplitude per incident angle which will lead to unambiguous angular detection of incident sound. From the difference over sum plot in Figure 43, the sensor designed with a 150 µm radius hole in the back plate can provide a range of detection from $-90° \leq \theta \leq 90°$ with a nearly linear sensitivity of ± 0.8, the highest difference over sum sensitivity achieved within this study. By enclosing the cavity behind the sensor and controlling the size of back plate hole, we have successfully designed a sensor that can detect an incident signal over a 180° range without left and right ambiguity.

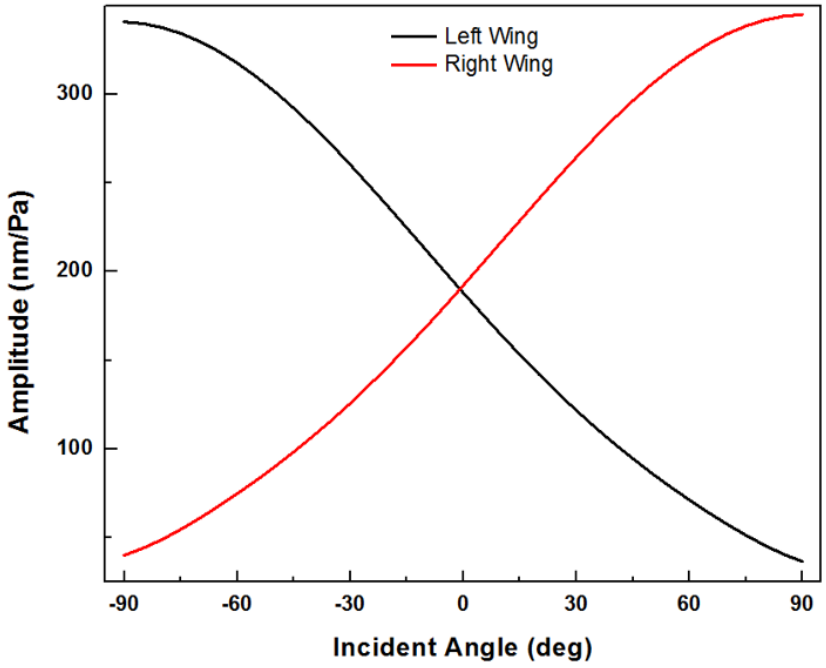

Figure 42. Angular Dependence at 1140 Hz with 150 µm Radius Hole in Back Plate

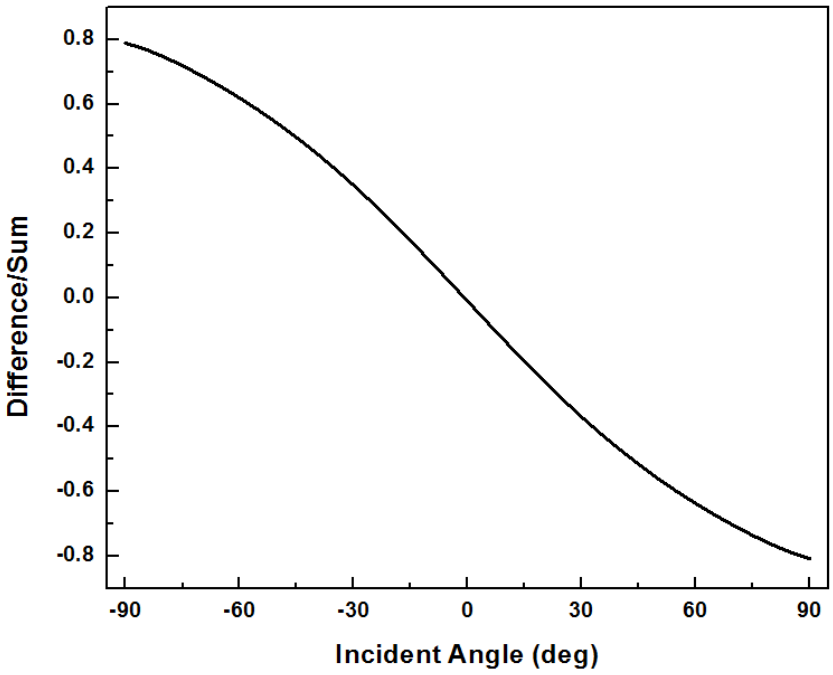

Figure 43. Difference Over Sum Using the Simulated Data in Figure 42

V. CONCLUSIONS

A. SUMMARY OF RESULTS

The *Ormia ochracea* parasitic fly is able to determine the incident angle of a cricket chirp by coupling the natural oscillation modes of its hearing organ. Many previous designs of *Ormia*-based direction finding MEMS acoustic sensor have exploited just one of the natural oscillation modes or performed a cursory study of the coupling between the two modes that was limited, to some extent, by sensor readout electronics. Furthermore, very few studies analyzed the response of a MEMS acoustic sensors when the backside air cavity was closed or restricted. This work aimed to study and design an *Ormia*-based sensor capable of unambiguously detecting incident sound over 180 degrees by using the displacement amplitude independently measured from both wings. The angle of the incident sound is proportional to the difference over the sum of these amplitudes.

Finite element modeling and simulation was extensively used to understand the overall behavior of the sensor under different constraints. With open back, the sensor behaves as a pressure gradient microphone therefore the predominant mode of oscillation is bending. In this condition it was not possible to obtain unambiguous angular detection over a full hemisphere (180°). In the opposite case, where the backside is completely sealed, the bending oscillations are almost completely suppressed and, again, the determination of the direction of the incident sound suffered from ambiguities.

Sophisticated experimentation was performed on several sensors, pre-designed with no specific requirement. This was performed to validate the FE models, used as a design platform for the optimized sensors to be fabricated in the future. Synchronous demodulation, using lock-in amplifiers, was the technique of choice to obtain an electric signal proportional to the amplitude of oscillations of the wingtips. The difference over the sum ratio was obtained by post possessing the data. Configurations similar to the simulations were experimented and the results were in good agreement, validating the design model.

Finally, using the developed FE model, a combination sensor/cavity was created to fulfill the desired requirement. By using a sensor with similar characteristics of the ones on hand and controlling the cavity by closing the back of the sensor and allowing some air to leak through a small aperture, the full range of angular detection was achieved.

This study demonstrated an important advancement in this sensor technology by simultaneously measuring and utilizing the superposition between the rocking and bending natural oscillation modes to determine the incident direction of a sound source. The amplitude of the rocking and bending mode present at a given frequency determines the overall superposition or coupling between the two types of the oscillations, which allows for the determination of the directional response at that frequency. In order to control the amplitude at which the bending oscillation is present at the rocking frequency, the air cavity behind the sensor was physically restricted. This generates a resistive force on the backside of the sensor wings.

Sealing the backside cavity completely damped out the bending mode. This led to high directional sensitivity over a small range of angles, proving that both modes are required to determine the incident direction of a sound source over a wide range. By creating an aperture in the backside of the closed sensor cavity, the bending mode FWHM is broadened and the peak shifts towards the rocking mode, affecting the superposition of the wings. When the backside cavity of the sensor was appropriately designed by optimizing the backside aperture through FE simulations, unambiguous determination of incident sound over a 180° range was achieved with maximum sensitivity.

For Department of Defense applications, the ability to detect an incident sound source over a full 180° range with just a single sensor drastically reduces the form factor of the overall device and significantly reduces power consumption. By altering the geometry of the sensor, the device can be tuned to detect a specific frequency of concern, thereby allowing it to be implemented for numerous applications.

B. RECOMMENDATIONS FOR FUTURE WORK

This study is merely a small stepping stone in a long line of developments that have been made in sound sensors based off of the *Ormia* fly. As this research progresses, the

goal is to manufacture sensors and form-factors that minimize size and maximize sensitivity and directional detection.

When the new sensors are fabricated and received, they will need to be fully characterized to compare with simulated the directionality in this study. It is recommended that a follow-on study be to test the sensor with an array of back plate holes with different radii to study the effects of this hole on the range of angular detection.

Although the electronics used in this study allow for simultaneous detection of the deflection of both wings individually, there is significant post-processing of the data that must be done to achieve the angular response and difference over sum readout. Circuitry and software that is able to produce real-time bearings to the incident direction of sound should be implemented. This will then allow for design of a wearable form-factor for field testing and Department of Defense applications.

THIS PAGE INTENTIONALLY LEFT BLANK

LIST OF REFERENCES

[1] R. N. Miles, D. Robert and R. R. Hoy, "Mechanically coupled ears for directional hearing in the parasitoid fly Ormia ochracea," *J. Acoust. Soc. Am.*, vol. 98, no. 6, pp. 3059–3070, Dec. 1995. [Online]. https://doi.org/10.1121/1.413830

[2] A. Ishfaque and B. Kim, "Fly ormia ochracea inspired mems directional microphone: a review," *IEEE Sensors Journal*, vol. 18, no. 5, pp. 1778–1789, 2018. [Online]. https://doi.org/10.1109/jsen.2017.2787862

[3] W. Cui, B. Bicen, N. Hall, S. A. Jones, F. L. Degertekin and R. N. Miles, "Optical sensing in a directional mems microphone inspired by the ears of the parasitoid fly, Ormia Ochracea," *19th IEEE International Conference on Micro Electro Mechanical Systems*, Istanbul, Turkey, 2006. [Online]. https://doi.org/10.1109/memsys.2006.1627874

[4] H. Liu, L. Currano, D. Gee, T. Helms and M. Yu, "Understanding and mimicking the dual optimality of the fly ear," *Scientific Reports*, vol. 3, p. 2489, 2013. [Online]. https://doi.org/10.1038/srep02489

[5] D. J. Mackie, J. C. Jackson, J. G. Brown, D. Uttamchandani and J. F. C. Windmill, "Directional acoustic response of a silicon disc-based microelectromechanical systems structure," *Micro & Nano Letters*, vol. 9, no. 4, pp. 276–279, 2014. [Online].

[6] MEMSCAP, "MEMSCAP: SOIMUMPS and MEMS Multi Project Wafer Service." Accessed January 22, 2020. [Online]. Available: http://www.memscap.com/products/mumps/soimumps.

[7] R. H. Downey and G. Karunasiri, "Reduced residual stress curvature and branched comb fingers increase sensitivity of MEMS acoustic sensor," *Journal of Microelectromechanical Systems*, vol. 23, no. 2, pp. 417–423, 2014. [Online]. https://doi.org/10.1109/jmems.2013.2279017

[8] D. Wilmott, "Direction finidng using multiple MEMS acoustic sensors," M.S. thesis, Dept of Physics, NPS, Monterey, CA, 2015. [Online]. Available: http://hdl.handle.net/10945/47345

[9] W. D. Swan, "Bio-inspired MEMS direction finding acoustic sensor for air and underwater applications," M.S. thesis, Dept of Physics, NPS, Monterey, CA, 2016.

[10] D. Wilmott, F. Alves and G. Karunasiri, "Bio-inspired miniature direction finding acoustic sensor," *Scientific Reports*, vol. 6, 2016. [Online]. https://doi.org/10.1038/srep29957

[11] M. Touse, J. Sinibaldi, K. Simsek, J. Catterlin, S. Harrison and G. Karunasiri, "Fabrication of a microelectromechanical directional sound sensor with electronic readout using comb fingers," *Applied Physics Letters*, vol. 96, no. 17, 2010. [Online]. https://doi.org/10.1063/1.3418640

[12] R. Parminder, "Design and testing of bio-inspired MEMS direction-finding acoustic sensors," M.S. thesis, Dept of Physics, NPS, Monterey, CA, 2018.

[13] COMSOL, Burlington, MA, USA. 2018. COMSOL Multiphysics, ver. 5.4. Available: https://www.comsol.com/

[14] R. Rabelo, F. Alves and G. Karunasiri, "Electronic phase shift measurement for the determination of acoustic wave DOA using single MEMS biomemtic sensor," unpublished.

INITIAL DISTRIBUTION LIST

1. Defense Technical Information Center
   Ft. Belvoir, Virginia

2. Dudley Knox Library
   Naval Postgraduate School
   Monterey, California